RMetS
Royal Meteorological Society

Assessing the performance of a prognostic and a diagnostic cloud scheme using single column model simulations of TWP–ICE

Charmaine N. Franklin,[a]* Christian Jakob,[b] Martin Dix,[a] Alain Protat[a,c] and Greg Roff[a]

[a]*Centre for Australian Weather and Climate Research – A partnership between CSIRO and the Australian Bureau of Meteorology*

[b]*School of Mathematical Sciences, Monash University, Australia*

[c]*Laboratoire ATmosphère, Milieux, Observations Spatiales, Vélizy, France*

*Correspondence to: C. N. Franklin, CSIRO Marine and Atmospheric Research, Private Bag No. 1, Aspendale, Victoria 3195, Australia. E-mail: charmaine.franklin@csiro.au

Single column model simulations using the UK Met Office Unified Model, as used in the Australian Community Climate Earth System Simulator, are presented for the Tropical Warm Pool–International Cloud Experiment (TWP–ICE) field study. Two formulations for the representation of clouds are compared with the extensive observations taken during the campaign, giving insight into the ability of the model to simulate tropical cloud systems. During the active monsoon phase the modelled cloud cover has a stronger dependence on relative humidity than the observations. Observed ice cloud properties during the suppressed monsoon period show that the ice water content is significantly underestimated in the simulations. The profiles of modelled ice fall speeds are faster than those observed in the levels above 12 km, implying that the observations have smaller sized particles in larger concentrations than the models. Both simulations show similar errors in the diurnal cycle of relative humidity during the active monsoon phase, suggesting that the error is less sensitive to the choice of cloud scheme and rather is driven by the convection scheme. However, during the times of suppressed convection the relative humidity error is different between the simulations, with congestus convection drying the environment too much, particularly in the prognostic cloud-scheme simulation. This result shows that the choice of cloud scheme and the way that the cloud and convection schemes interact plays a role in the temperature and moisture errors during the suppressed monsoon phase, which will impact the three-dimensional model simulations of tropical variability. Copyright © 2011 Royal Meteorological Society

Key Words: TWP–ICE; cloud parametrization; tropical convection

Received 18 April 2011; Revised 9 August 2011; Accepted 27 September 2011; Published online in Wiley Online Library 7 November 2011

Citation: Franklin CN, Jakob C, Dix M, Protat A, Roff G. 2012. Assessing the performance of a prognostic and a diagnostic cloud scheme using single column model simulations of TWP–ICE. *Q. J. R. Meteorol. Soc.* **138**: 734–754. DOI:10.1002/qj.954

1. Introduction

The Tropical Warm Pool–International Cloud Experiment (TWP–ICE) was a major field campaign held in the Darwin area in northern Australia in January and February 2006 (May *et al.*, 2008). One of the main aims of the experiment was to provide boundary conditions and validation data for modelling studies to help facilitate model development with

a focus on tropical convection and clouds. The Darwin area experiences a wide array of convective systems consisting of active monsoon periods with typical maritime storms and break periods with more coastal and continental convection (Keenan and Carbone, 1992). The observations collected during the TWP–ICE campaign allow for a detailed evaluation of the ability of numerical models to simulate the evolution of tropical cloud systems and their effect on the environment. Global climate models (GCMs) must be able to represent cloud-scale processes and the feedbacks between clouds and the large-scale environment to ensure accurate projections of climate change.

Single column models (SCM) are useful tools in the evaluation and development of atmospheric physical parametrizations in numerical models (e.g. Randall *et al.*, 1996). The SCM represents a vertical column in a GCM and calculates the temporal evolution of the vertical profiles of temperature and moisture as well as that of many subgrid-scale variables, such as clouds and radiation. The advection by the large-scale flow is prescribed and the errors produced by the model's physical parametrizations will be reflected in the temperature and moisture fields as well as in the parametrized variables themselves. An advantage of the SCM approach is that by keeping the large-scale atmospheric circulation close to observations, a better assessment of the physical parametrizations is enabled. Single column models provide a simple, inexpensive means to identify parametrization errors and inadequacies, however, care needs to be taken in the interpretation of the SCM evaluation as the errors seen in the SCM may not be the same as those in the full three-dimensional GCM due to the lack of feedbacks between the subgrid- and grid-scale processes in the SCM. If the SCM forcing data are realistic then the SCM may produce smaller biases than the GCM. However, because there is no feedback to the larger scales in the SCM simulation, the biases could grow with time and become larger than those of the full GCM (see e.g. Bergman and Sardeshmukh, 2003).

The primary aim of the work presented here is to use the SCM approach with a version of the UK Met Office SCM to assess the ability of two fundamentally different parametrizations of clouds to reproduce the observed thermodynamic and cloud structures as well as the associated radiative fluxes during the TWP–ICE experiment. The two model versions used are based on the UK Met Office Unified Model (MetUM), whereby one version uses a new generation prognostic cloud scheme (Wilson *et al.*, 2008a) while the other employs the current (or control) diagnostic scheme used routinely in the model (Smith, 1990). The results presented here complement the study of Wilson *et al.* (2008b) who compared the same two representations of clouds using climate simulations. The next section will describe the model and the forcing and validation data used in this study. Section 3 describes the general characteristics of the TWP–ICE meteorology and discusses the model performance for two of the weather regimes that occurred during the campaign. Section 4 presents a detailed validation of the simulated cloud cover and section 5 evaluates the ice cloud properties simulated by the cloud schemes. A summary of the findings is discussed in section 6.

2. Experiment design

The Australian Community Climate Earth System Simulator (ACCESS) is a new coupled climate and earth system model that is being developed as a joint initiative between the Australian Bureau of Meteorology and the Commonwealth Scientific and Industrial Research Organisation (CSIRO) in partnership with Australian universities. The model provides a framework for numerical weather prediction and studies of climate change and enables research into processes occurring in the Earth system. (For information on the modelling system see http://www.accessimulator.org.au/) The atmospheric component of ACCESS is the MetUM and throughout this paper the model will be referred to as the ACCESS model. As part of the ACCESS project this model needs to be extensively validated in the Australian region. One of the experiments designed to evaluate the ACCESS atmospheric model in the Australian region is to run the SCM for the TWP–ICE case. This intensive field campaign has produced a dataset for model evaluation that provides a good test for the parametrizations within GCMs, such as the ACCESS model.

2.1. Description of the ACCESS/MetUM single column model

The ACCESS SCM used in this study is the MetUM version 7.1 with 38 vertical levels, and is based on the second version of the Hadley Centre Global Environment Model (HadGEM2) described in Collins *et al.* (2008). The large-scale cloud scheme used in the model is described by either the diagnostic scheme of Smith (1990) with modifications (Wilson *et al.*, 2004) or a new prognostic cloud scheme (Wilson and Bushell, 2007; Wilson *et al.*, 2008a); note that the ice condensate is prognostic in both schemes. The cloud fraction from the simulation using the diagnostic scheme is the sum of the cloud fraction from the large-scale cloud scheme of Smith (1990) and a diagnostic convective cloud fraction described by Gregory (1999). The new prognostic cloud scheme that has been developed for the MetUM includes prognostic variables for the cloud liquid-water content, the cloud ice-water content, the bulk cloud fraction, the liquid cloud fraction and the ice cloud fraction. Diagnostic cloud schemes such as the Smith (1990) scheme are relatively simple in their representation of cloud properties and exhibit strongly constrained relationships between cloud variables. These relationships restrict the variability of the cloud fields and can produce unrealistic cloud properties (Wilson *et al.*, 2008a). The new PC2 cloud scheme (prognostic cloud, prognostic condensate) was designed to be more realistic by allowing a greater number of degrees of freedom in the cloud variables.

When the PC2 scheme is used several changes are made to the parametrization of the convective updrafts. The first is an increase in the proportion of condensate that is detrained high in the convective plumes, rather than being precipitated. The second change is a reduction of the phase-change temperature between liquid and ice condensate in the convective updrafts. In the PC2 simulation this temperature is reduced from the control value of 0°C to −10°C. These changes have been found to be necessary to produce realistic anvil clouds due to the direct interaction of the large-scale cloud variables in PC2 with the convection scheme (see Wilson *et al.* (2008b) for more details on these changes).

2.2. The TWP–ICE forcing and validation data

The large-scale single-column model forcing and evaluation dataset for TWP–ICE was derived by Xie *et al.* (2010) from the constrained variational objective analysis approach described in Zhang and Lin (1997). The aim of the objective analysis is to make minimum adjustments to the original sounding data to constrain the wind, temperature and humidity fields to satisfy conservation of mass, moisture, energy and momentum through a variational technique. The constraint variables used are surface pressure, surface latent and sensible heat fluxes, wind stress, precipitation, net radiation at the surface and top of the atmosphere, and variability of total column water content. The method takes into account measurement uncertainties in the radiosonde data and it has been shown that the magnitude of the adjustments required to meet conservation is comparable to these uncertainties (Zhang and Lin, 1997).

The domain used in the objective analysis covers an area of roughly 150 km in radius centred on Darwin. Within this area there were five boundary sounding stations that measured the vertical profiles of temperature, relative humidity and winds every 3 h during the intensive observation period. At the Atmospheric Radiation Measurement (ARM) Darwin site, which is at the centre of the analysis domain, soundings were available four times a day. The original soundings had a dry bias that has been corrected by Hume (2007). The amount of missing data range from 5 to 30% for the five boundary sounding sites, with the largest amount of missing data occurring for the soundings taken from the ship (Xie *et al.*, 2010). The variational analysis also required domain-averaged surface and top of the atmosphere measurements and these were provided by the Australian Bureau of Meteorology polarimetric and weather radar data (Keenan *et al.*, 1998), surface radiative and turbulence fluxes from the ship and land stations, surface meteorological fields from both the local mesonet and sounding stations, cloud liquid-water path from the ARM site and the ship, and satellite data from the Multi-functional Transport Satellite (MT-SAT). Any missing observations that the variational analysis needed were provided by the European Centre for Medium-Range Weather Forecasts (ECMWF) model data, where these data were adjusted using the linear regression equations that were derived at times when observations were available (Xie *et al.*, 2010).

The model is initialized once on 19 January 2006 and then run for 25 days. The observational forcing dataset has a temporal resolution of 3 h and this has been interpolated to the model time step of 30 min. The lower boundary condition used in the SCM experiments is a prescribed sea-surface temperature and the model calculates the turbulent fluxes of sensible and latent heat at the surface. This method is preferred to the prescription of turbulent surface fluxes as it allows the model to develop some feedback between the thermodynamic structure of the atmosphere and the surface heat and moisture exchange. However, as the experiment domain contains a mixture of land and ocean, this approach limits the usefulness of the results to periods that were not dominated by strong diurnal forcing due to local topography. This means that results towards the end of the simulation must be treated with caution, as convection during the break period is primarily initiated on circulations driven by local topography (e.g. sea breezes; May *et al.*, 2008). Three-dimensional advective tendencies are specified as forcing from the variational objective analysis and the model horizontal wind fields are relaxed back to those observed using a 3 h relaxation time-scale. We chose not to nudge the temperature and moisture fields for two reasons: nudging can mask errors from the model physics that affect temperature and humidity (Ghan *et al.*, 1999), and nudging these fields can also change cloud morphology through the elimination of radiative feedbacks on cloud formation (Menon *et al.*, 2003). As one of the aims of this study is to examine the different effects of the diagnostic and prognostic cloud schemes on both the cloud and radiative fields as well as the state variables of temperature and humidity, nudging these variables was deemed unsuitable. All cloud fields in the model are initialized to zero and some spin-up over the first few hours of the simulation is unavoidable. Due to a lack of observations, advection of cloud fields is not included in the simulations.

3. Model evaluation

This section provides a general overview of the model simulations highlighting some of the model behaviour with the different treatments of cloud. A more in-depth analysis of the simulated cloud fields will then be carried out in sections 4 and 5. The Darwin ARM site has a suite of active remote sensing instruments that provide vertical cloud structure information. The Active Remotely Sensed Cloud Layers (ARSCL) data have been provided as part of the TWP–ICE validation dataset and give information on the location of cloud layers (see Clothiaux *et al.* (2000) for details). The observations have been interpolated to the 38 model vertical levels and the horizontal winds have been used with a horizontal grid box size of 300 km to calculate the appropriate averaging time-scale as described by Protat *et al.* (2010). Sensitivity tests varying the size of the domain for these calculations showed little influence on the resulting cloud fractions. The observed cloud cover is shown in Figure 1 along with the cloud fraction from the two model simulations. The observations show that four meteorological regimes were observed during TWP–ICE. As discussed by May *et al.* (2008) TWP–ICE was initially characterized by an active monsoon period from 19 January to 25 January 2006, with deep convective clouds observed on all days. This period was followed by a suppressed monsoon phase until 2 February, characterized by relatively shallow convection with convective cloud tops <8 km and extensive cirrus. After a few clear days the regime shifted to the break monsoon period from 6 February (Julian day 37) where the convection was dominated by intense afternoon thunderstorms and squall lines.

The strong forcing associated with the deep convection during the active monsoon phase produces average surface rain rates of 17 mm day^{-1} and there is little deviation between the observed and modelled precipitation rates (not shown). This is to be expected as the use of precipitation as a constraint in the generation of the forcing dataset will produce upward motion at the times of rainfall. During the active monsoon phase both models show reasonable agreement with the cloud cover observations, but there are notable differences between the modelled and observed cloud fields. Initially the diagnostic cloud scheme produces clouds that extend higher than the observations and those produced by the prognostic scheme PC2. Neither scheme

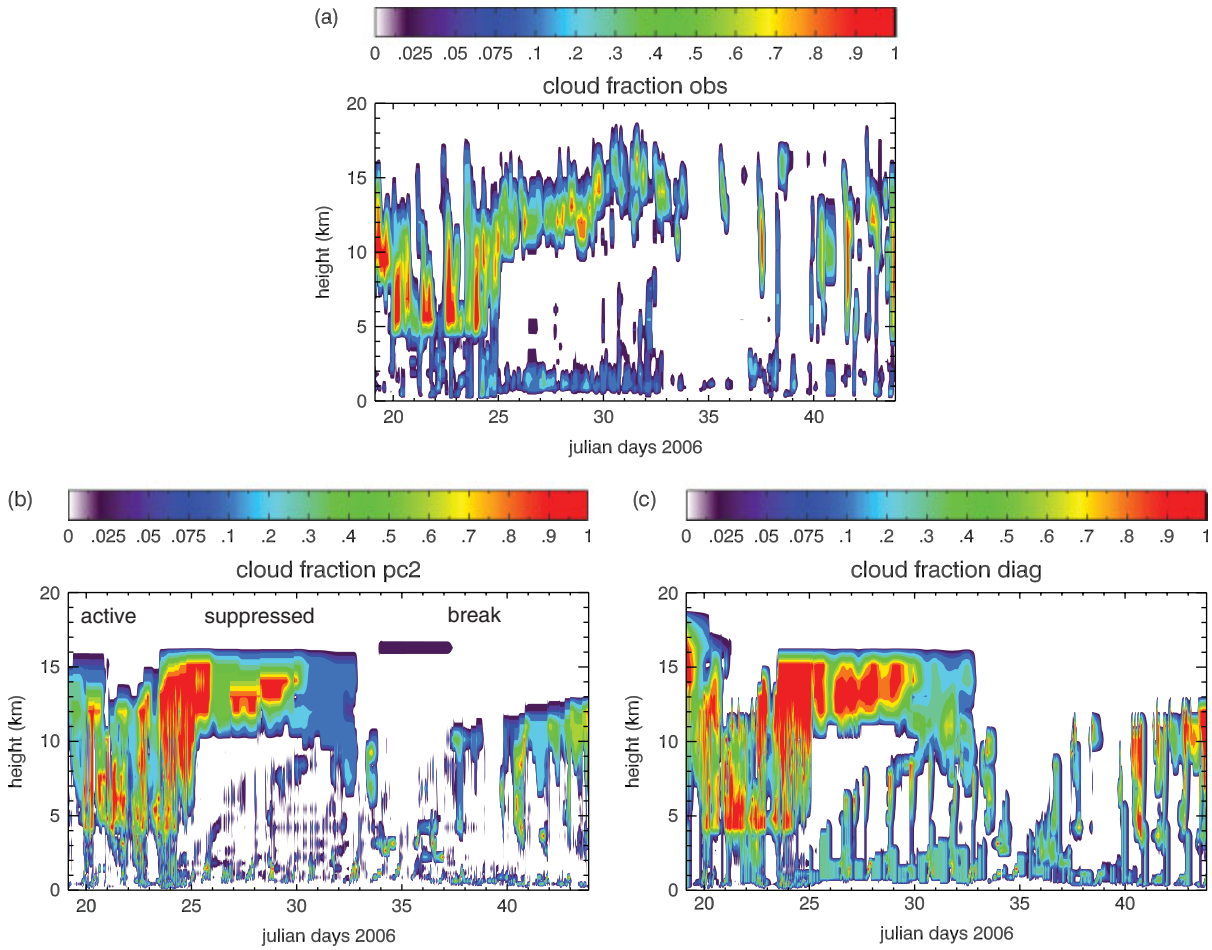

Figure 1. Cloud or hydrometeor fraction: (a) observed, (b) single column model (SCM) with PC2 cloud scheme and (c) SCM with diagnostic cloud scheme.

reproduces the reduction of cloud fraction with height seen in the observations, particularly the results from the diagnostic scheme. The lack of clear sky in the simulations during the active phase is apparent as are the lower cloud-top heights after 21 January. On 24–25 January when a mesoscale convective system was present in the experiment domain, both models produce similar cloud fractions that are much larger than those observed by the radar and lidar above 10 km. Given that the cloud radar had degraded sensitivity during TWP–ICE due to an earlier lightning strike (May *et al.*, 2008), satellite retrievals of cloud-top temperature from MT-SAT have been analysed for a 300 km horizontal domain centred on the radar site. For the first half of 24 January clouds with cloud-top temperatures between −70 and −90°C covered 40–63% of the domain, which is about 10% larger than the radar–lidar retrievals for clouds at 14–15 km that have three-hourly averaged cloud cover between 27 and 55%. At these times the overestimate the cloud cover with maximum values at these heights >95%. After this time both the radar–lidar and satellite derived cloud cover observations show reduced high cloud cover, while the models continue to produce cloud cover at 14–15 km >90% for the remainder of the active monsoon phase.

During the suppressed monsoon phase from 26 January the cloud structure changed from being characterized by the deep convective clouds of the preceding active monsoon phase, to shallow and occasional mid-level convective clouds topped by an extensive high-level cloud shield (Figure 1). During this phase the mean rainfall over the TWP–ICE domain was much lower than during the active monsoon period. The cumulative surface precipitation from the models over the suppressed phase is 5 mm greater than the 19 mm observed (not shown). The top and base of the cirrus cloud during the suppressed phase is initially well modelled, however, after Julian day 30 the observations show the cloud gradually rising and this is not captured by the model using either of the cloud schemes. During the suppressed phase of the simulations there is a warm bias in the levels above 12 km. The warming is a response to the radiative heating due to the lack of forcing above 16 km. Similar to Woolnough *et al.* (2010) and others no large-scale forcing is applied above 150 hPa due to uncertainties in the forcings at high altitudes. Results from a climate model study by Boyle and Klein (2010) that used operational analyses to run short-term forecasts for TWP–ICE, showed a substantial warm bias above 200 hPa during the suppressed phase compared with the heating profiles derived from the same variational analysis used here to force the SCM, suggesting that there may be imbalances in the large-scale forcings at upper levels. The prognostic cloud scheme reduces the cirrus cloud cover too much after day 30 compared with the observations and the diagnostic scheme (Figure 1). The diagnostic scheme produces more shallow cloud cover than is observed, as well as mid-level clouds with tops <8 km. These clouds continue to be present more in the simulation with the diagnostic scheme compared with the observations and the

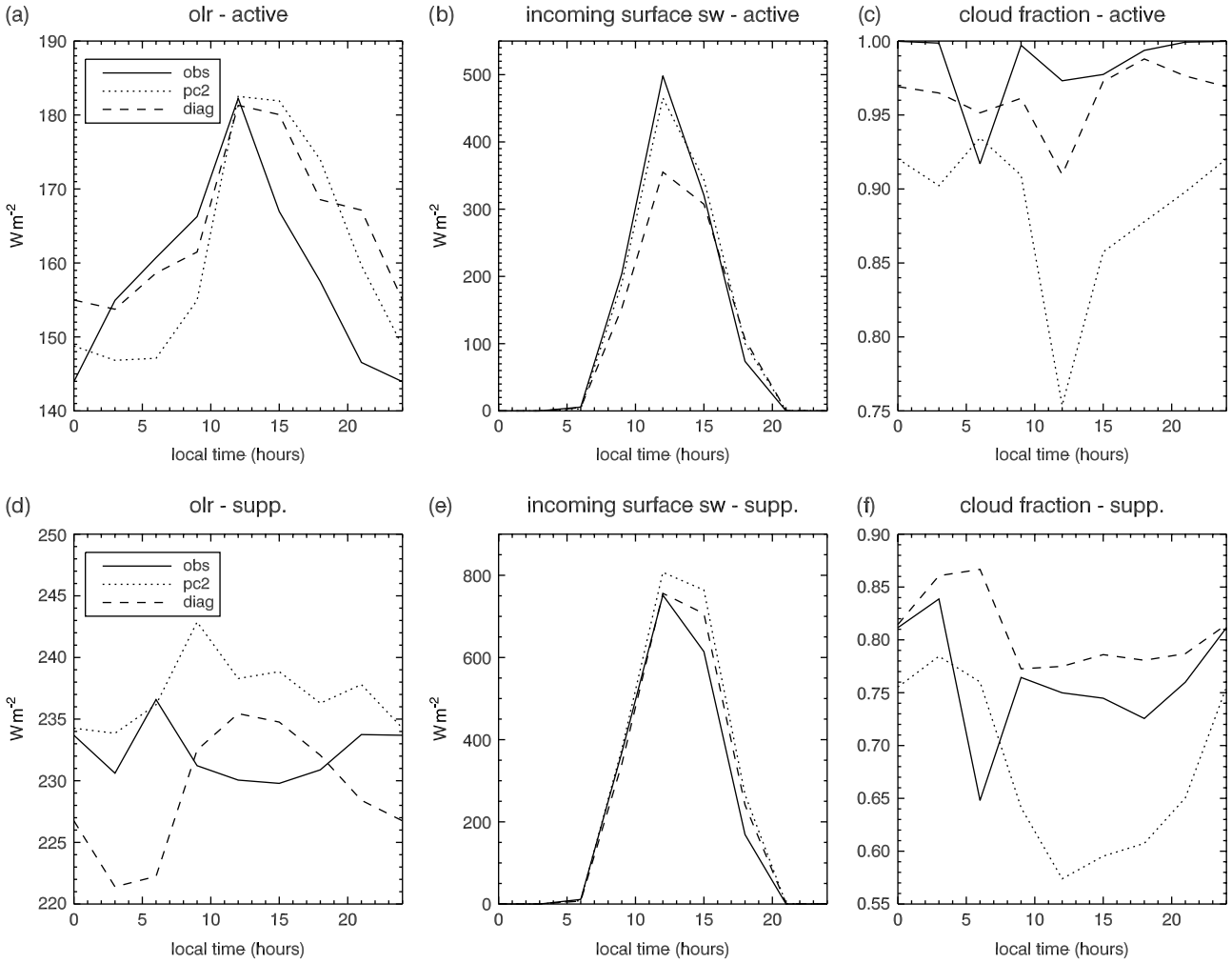

Figure 2. Average diurnal cycle during the (a) active monsoon phase of observed/analysed and simulated outgoing longwave radiation at the top of the atmosphere (W m^{-2}), (b) incoming solar radiation at the surface (W m^{-2}) and (c) total column cloud fraction. Observed values are shown by the solid line, those from the simulation with the PC2 cloud scheme are shown as the dotted line and the dashed line shows the results from the simulation with the diagnostic cloud scheme. (d)–(f) Same as (a)–(c) except for the suppressed monsoon phase.

PC2 simulation when the suppressed phase of TWP–ICE transitioned into a few clear days before the break period.

The monsoon break period is a difficult period to simulate with a SCM. In the observations this period was characterized by continental and coastal convection generated from sea breezes, resulting in strong but local convective events. As the processes forming sea breezes and the resulting convection are not included in SCMs, the models cannot be expected to simulate the associated cloud fields realistically. If they do so, this will most likely be an artefact of the forcing dataset, which through the use of precipitation as a constraint will produce mean upward motion at large scales at the time of rainfall, when it is clear from the observations that this motion was strongly focused in coastal and island sea breezes (see May *et al.*, 2008). For the reasons above we refrain from an in-depth discussion of the results for this period.

3.1. The active monsoon period (Julian days 19–24)

After providing an overview of the general model performance, we will now analyse the model behaviour for the active and suppressed (section 3.2) monsoon periods observed during TWP–ICE. Radiation fields can be used to evaluate the combined effects of the cloud layers on the absorption and reflection of the solar and infrared radiation. Figure 2(a) shows the average diurnal cycle over the active period of outgoing long-wave radiation (OLR) at the top of the atmosphere. The simulations capture the trend shown in the observations of OLR increasing throughout the morning and decreasing after the onset of convection in the afternoon. In general the sign of the biases shown by both models is the same, with too little OLR in the morning and too much in the afternoon and evening. The simulation with the prognostic scheme is better able to maintain high cloud around the local midnight hours compared with the diagnostic scheme and produces a better amplitude in the diurnal cycle of OLR, however, PC2 does not clear cloud fast enough throughout the morning. The total column cloud amount as seen from above is calculated from the simulations using the assumption of a maximum randomly distributed cloud field (i.e. maximum overlap of adjacent but random overlap of separate cloudy layers). Both simulations produce lower total column cloud cover (Figure 2(c)) than is observed, particularly the prognostic scheme, for which cloud cover at times is 20% lower than observed. This underestimate of cloud cover contributes to the OLR error during the latter half of the day.

The times when both of the models agree well with the observed OLR is at noon and it is at this time when the relative humidity bias from both simulations is the

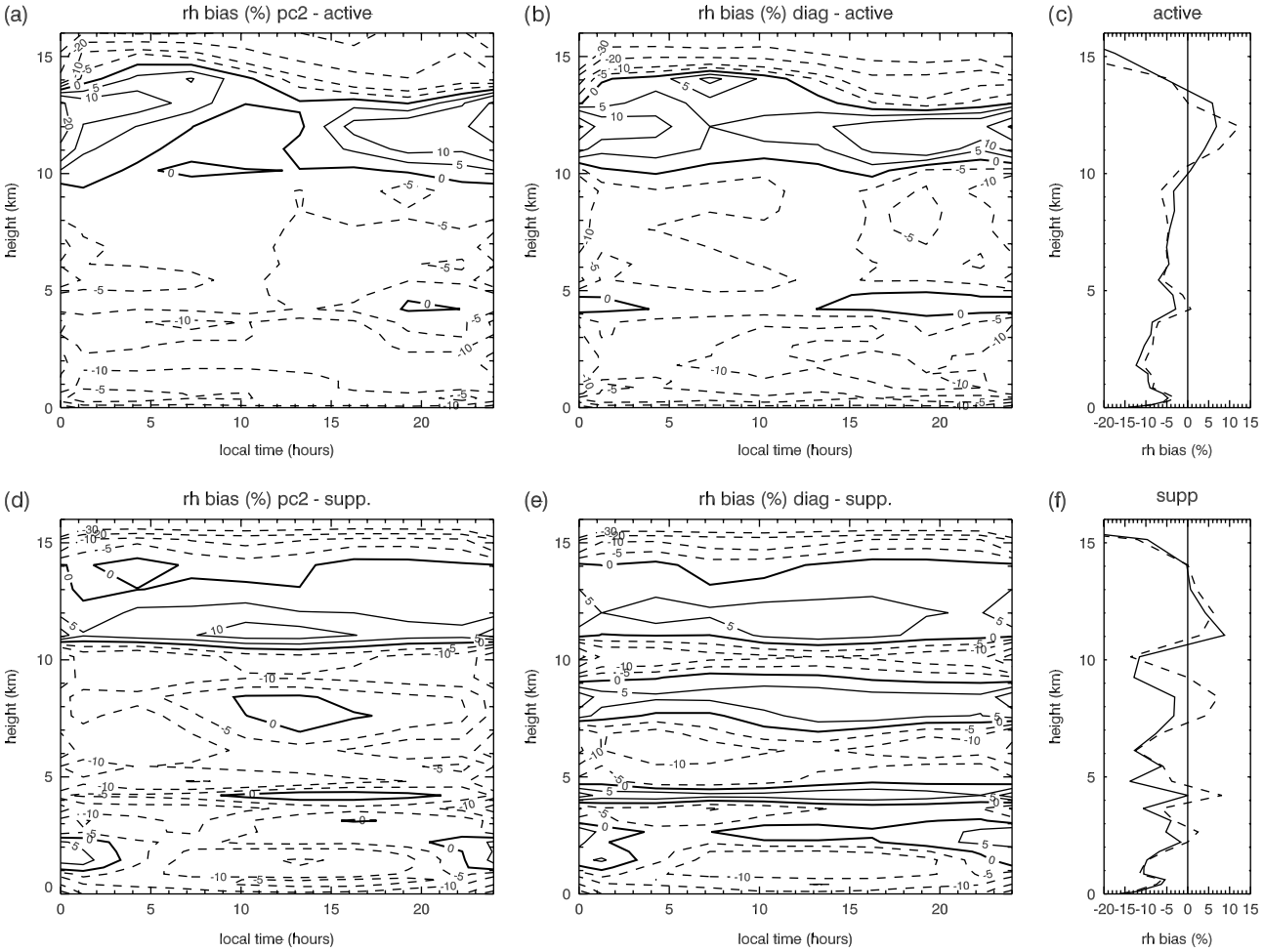

Figure 3. Diurnal cycle of relative humidity (%) bias for the active (a, b) and suppressed (d, e) monsoon phases for the simulation with the PC2 cloud scheme (a, d) and the diagnostic cloud scheme (b, e). The average profiles of relative humidity for the (c) active and (f) suppressed phases for the prognostic (diagnostic) cloud scheme simulation in the solid (dashed) lines.

lowest in the upper levels (see Figure 3). During the active monsoon phase both simulations produce generally similar biases in relative humidity. The diurnal cycle of the relative humidity biases show that when convection is triggered in the early afternoon, the upper levels of the convective clouds develop a positive bias with a negative bias below, and this relative humidity error structure persists into the early morning. The relative humidity bias produced in these SCM simulations has been documented in previous studies of active convection using the three-dimensional MetUM by Petch *et al.* (2007), where it was identified that the main cause of the bias was a sharp reduction in mass flux at the top of convective plumes. Improvements to the convection scheme reduced the bias, however, the vertical structure of the relative humidity error remained (Petch *et al.*, 2007). The reproduction of this bias gives credence to the use of this SCM methodology to examine the performance of the physical parametrizations in simulations of tropical convection.

The average diurnal cycle of incoming solar radiation at the surface during the active monsoon phase is generally well simulated by the prognostic cloud scheme (Figure 2(b)), while the diagnostic scheme underestimates the solar radiation at the surface by up to 150 W m^{-2}. From the afternoon into the early evening both of the models simulate too much incoming solar radiation at the surface. When convection becomes active in the early afternoon the levels below 4 km have the strongest negative relative humidity bias as shown in Figure 3, and this could be due to the convection being too efficient at drying these levels or not enough evaporation occurring from the stratiform rain to moisten the atmosphere. Other studies using the MetUM have noted deficiencies in the representation of cloud pools during active convection (Petch *et al.*, 2007; Willett *et al.*, 2008). The results of this study support the idea of Petch *et al.* (2007) that the downdrafts from deep convection in the model and their impact on the boundary layer plays a role in the temperature and moisture biases produced by the model in the low levels, which leads to errors in the surface radiation budget (Figure 2(a)).

Average temperature and moisture increments over the active monsoon period from each of the physical processes in the SCM and the observational/advective forcing are shown in Figure 4 for the two simulations with different cloud schemes. Convection is the dominant physical process in both simulations during this period of TWP–ICE, acting to warm and dry the atmosphere, opposing the cooling and moistening from the large-scale processes. The stratiform rain, driven by the microphysics of the stratiform cloud component, acts to cool and moisten the atmosphere below the freezing level (around 5 km height) through evaporation and melting, and warm and dry the levels above by condensation. Heating from short-wave radiation and long-wave cooling are largest from about 5–14 km. The

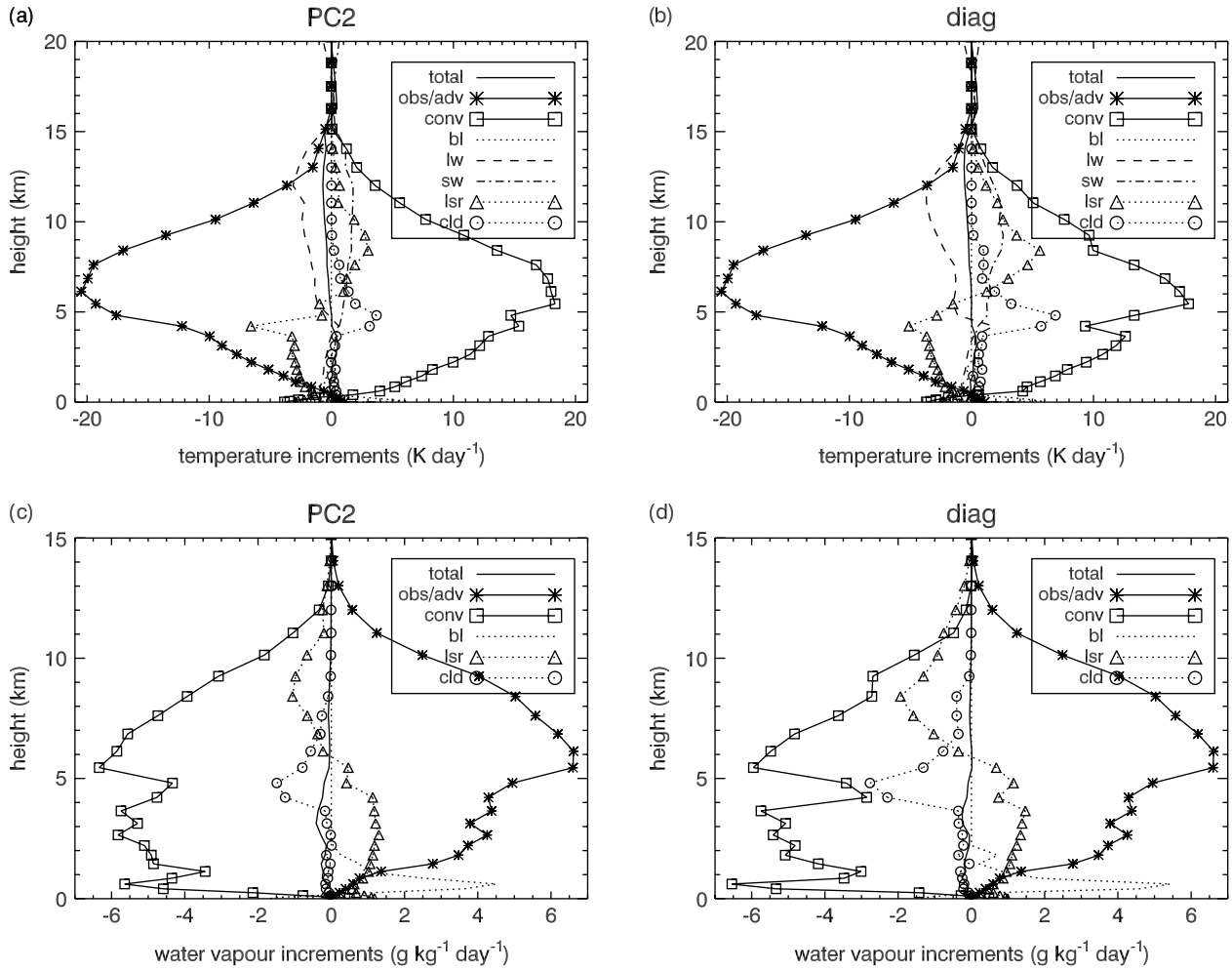

Figure 4. Average active monsoon phase (a) temperature (K day^{-1}) and (b) water vapour (g kg^{-1} day^{-1}) increments from the observations/analysis (advective tendencies, obs/anal), convection (conv), the boundary layer scheme (bl), the microphysics or large-scale rain scheme (lsr), the short-wave (sw) and long-wave (lw) radiation, the cloud scheme (cld) and the total increment for the simulation using the PC2 cloud scheme. (b) and (d) are for the diagnostic cloud-scheme simulation.

boundary layer transports warm, moist air from the surface to the lowest levels of the atmosphere and the condensational heating from the cloud schemes, which have contributions from each of the other budget components, is dominant at the freezing level, where vapour detrained from convective plumes is condensed into large-scale condensate.

The simulation using the prognostic cloud scheme has stronger tendencies from convection at the freezing level. At this level in both simulations the gradient of the convective heating and drying rate changes and reflects the large effect of detrainment as the buoyant air reaches the more stable layer near the melting level at about 5 km. The simulation with PC2 shows less of a change in the convection tendency profiles of temperature and vapour due to the effect of convective plumes detraining both vapour and condensate. While this change from convection is balanced mostly by the large-scale cloud temperature and moisture increments, there is a stronger dry bias at this level in the PC2 simulation (Figure 3). Although the boundary layer negative relative humidity bias is similar for both simulations, convective drying and boundary layer moistening is stronger in the run with the diagnostic scheme. The increased convection gives rise to greater cloud cover from the diagnostic scheme simulation and produces a larger underestimate of incoming solar radiation at the surface as compared with the PC2 simulation (see Figure 2(a)).

As was found by Wilson *et al.* (2008b) the average mass flux is reduced in the PC2 simulation compared with the diagnostic cloud-scheme simulation (see Figure 5(a)). However, when averaged over only the times when the deep convection scheme is active, the updraft mass flux from the PC2 simulation is larger between the boundary layer and 13 km during the active monsoon phase (Figure 5(c)). The reason for the reduced strength of convection in the upper troposphere is because the detrainment rates are increased between 10 and 13 km in the prognostic scheme simulation (not shown) due to the tuning of the convective precipitation function as discussed in section 2.1. During the active monsoon phase both deep and mid-level convection are not triggered as often in the prognostic cloud-scheme simulation. However, when there is convection the deep scheme produces larger mass fluxes and the increased mass flux averaged over all times from the diagnostic scheme simulation is due to the contributions from mid-level convection (Figute 5(d)). Willett *et al.* (2008) found that deep convection in the MetUM often terminated at levels too low and that resulted in mid-level convection acting on local instabilities that were not initiated from the surface. For this SCM case study, the larger mass flux from deep

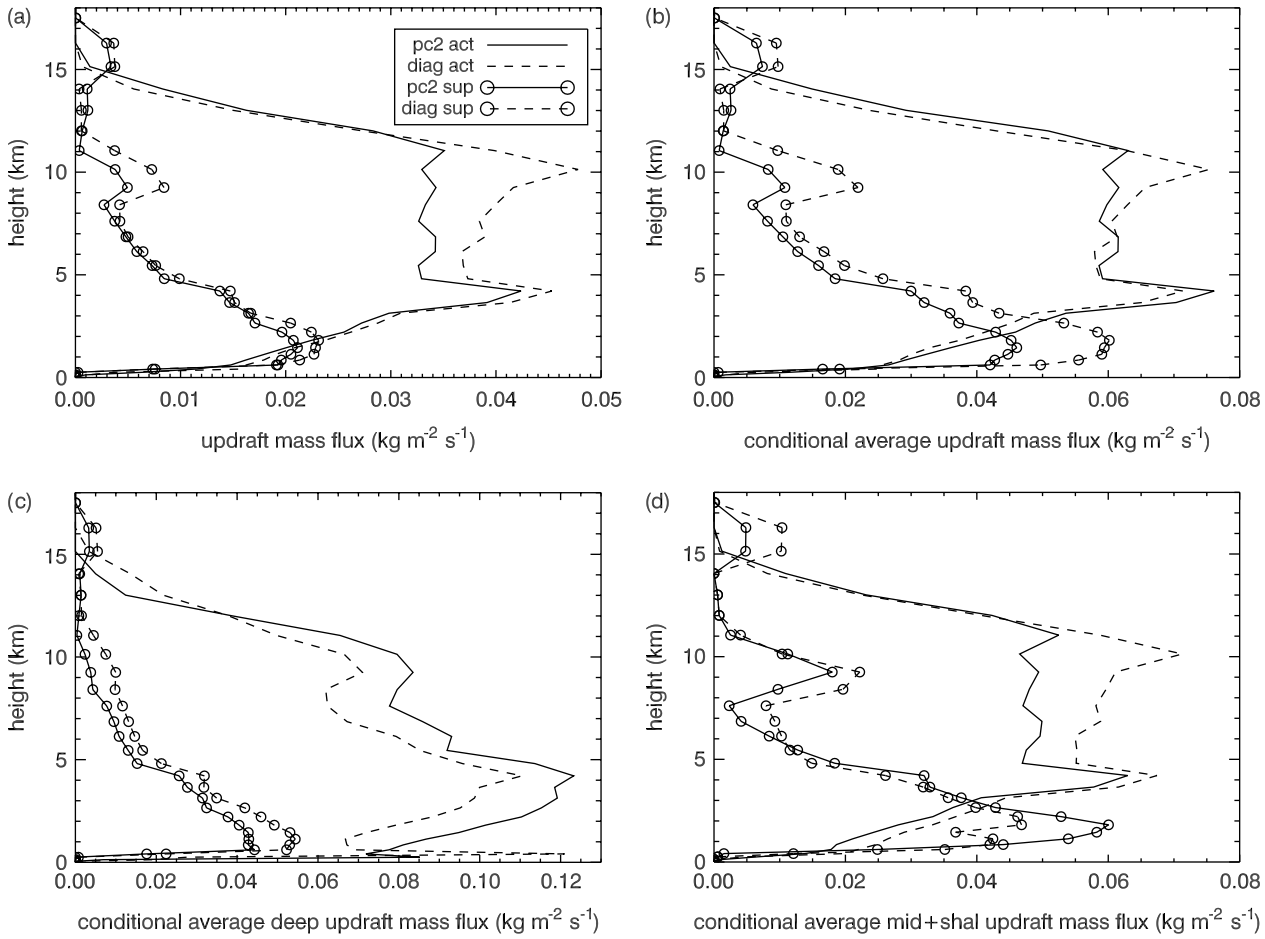

Figure 5. (a) Average updraft mass flux (kg m^{-2} s^{-1}) for the prognostic and diagnostic cloud-scheme simulations for the active monsoon phase (solid and dashed lines respectively) and the suppressed monsoon phase (solid and dashed lines with circles). (b) Average updraft mass flux over only those times when convection is active. (c) Average updraft mass flux over only those times when the deep convection scheme is active. (d) Average mass flux over those times when the mid-level and shallow convection schemes are active.

convection in the prognostic scheme simulation and the smaller mass flux from mid-level convection are arguably more realistic during this active monsoon phase.

The reduction in mass flux over the active phase in the PC2 simulation is due to changes in the thermodynamic structure of the atmosphere, with larger negative relative humidity biases below 6 km in this simulation (Figure 3). The less moist mid-lower troposphere limits the strength of convection as demonstrated by Derbyshire *et al.* (2004). The differences in temperature and moisture between the simulations during the active monsoon phase are primarily caused by the direct coupling between the prognostic cloud and convection schemes, where there is a change from the diagnostic cloud scheme to detrain condensate directly into the large scale and an associated tuning to allow more detrainment rather than convective precipitation. These changes produce similar average evaporation rates from the large-scale precipitation between the simulations (Figure 6(a)). Convective detrainment and evaporation are the two sources of moisture needed to balance the warming during the times of deep convection. Given the larger relative humidity bias this balance is achieved less in the prognostic cloud-scheme simulation.

The simulations have a cold bias of similar magnitude between 7 and 15 km where cloud ice concentrations are maximal. This cold bias has been documented in active convection studies with the global MetUM using the diagnostic cloud scheme, where it has been noted that the convection scheme does not warm enough to offset the radiative cooling (Willett *et al.*, 2008). Figure 4(a) shows that the model produces the same bias when the prognostic cloud scheme is used due to the counteracting changes in the long-wave cooling and convective warming increments during times of deep convection.

3.2. *The suppressed monsoon period (Julian days 25–35)*

The average diurnal cycle of OLR during the suppressed monsoon phase of TWP–ICE shows that the prognostic cloud scheme captures the increasing OLR in the early morning reasonably well, however, the OLR is increased too much into the later morning hours and remains higher than the observations for the remainder of the day (Figure 2(d)). The diagnostic cloud-scheme simulation on the other hand, underestimates the average OLR during the morning hours by up to 10 W m^{-2}, and similar to the prognostic scheme overestimates the OLR in the middle of the day. Both simulations produce greater amplitudes in the average diurnal cycle of OLR compared with the observations and often the gradient of the simulated diurnal cycle of OLR is opposite to that observed, particularly for the diagnostic scheme simulation. The lowest observed OLR occurs during the early afternoon, which coincides with the times of coldest cloud-top temperature observations from Tropical

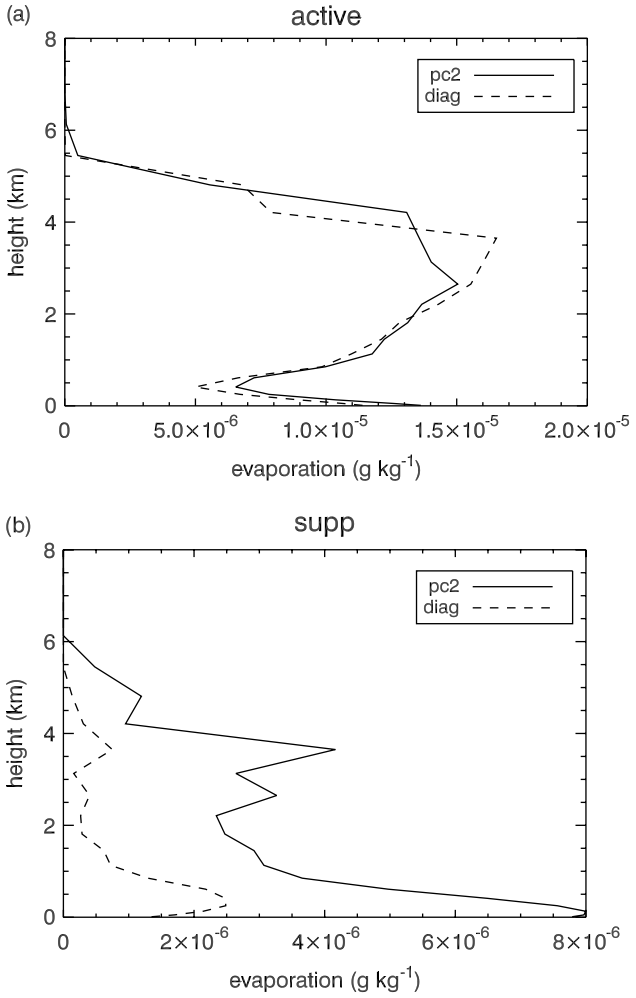

Figure 6. Average evaporation (g kg^{-1}) from the large-scale precipitation for the (a) active and (b) suppressed monsoon phases, with the prognostic (diagnostic) cloud-scheme simulation shown by the solid (dashed) lines.

Ocean Global Atmosphere Coupled Ocean–Atmosphere Response Experiment (TOGA COARE) for convectively suppressed tropical oceanic conditions (Chen and Houze, 1997). The representation of OLR and the incoming short-wave radiation in the afternoon is the least well captured in the simulation with PC2, which is shown to be at least partly caused by an underestimate of cloud cover of between 10 and 15%. The early morning is the time when the OLR error is the largest from the diagnostic scheme simulation, even though the total cloud cover at these times is in reasonable agreement with the observations (Figure 2(f)). This suggests that the simulated vertical distribution of cloud and/or the in-cloud water contents are different to those observed and these will be examined in the following sections.

The almost 20% reduction in observed cloud cover during the morning is simulated too late in the models, with the magnitude not reduced enough by the diagnostic scheme and too much by the prognostic scheme (Figure 2(f)). This reduced cloud cover in the PC2 simulation produces greater OLR and incoming solar radiation at the surface from late morning throughout the remainder of the day. The relative humidity errors shown in Figures 3(d) and (e) for the suppressed monsoon phase are negative in the levels below 10 km for the prognostic cloud-scheme simulation and vary in sign for the simulation using the diagnostic cloud scheme. During the suppressed phase there is greater temporal and vertical variability in the relative humidity errors than during the active monsoon phase. The largest difference in relative humidity between the simulations is between 4–5 and 7–9 km, where the sign of the bias differs, with the PC2 simulation producing the negative relative humidity bias.

The average temperature and moisture increments for the suppressed monsoon period are shown in Figure 7 for the two simulations. There is little difference in the increments between the simulations, except for PC2 having stronger average convective temperature tendencies in the low levels. The fact that this does not translate into greater cloud cover compared with the diagnostic scheme simulation is due to more of the shallow cloud drizzling away each time step in the PC2 simulation. This can be seen by the larger evaporation rates from the large-scale microphysics in the PC2 simulation compared with that from the diagnostic scheme simulation (Figure 6(b)). As discussed by Wilson *et al.* (2008b), the large in-cloud condensate amounts from convective detrainment in shallow convection allow for the efficient removal of cloud water through the generation of precipitation in the PC2 simulation. They found that with increased vertical resolution the reduction of liquid water by precipitation was decreased and instead it was the erosion term, which models the entrainment of dry air, that reduced the cloud water. For the TWP–ICE case study the enhanced precipitation in the PC2 simulation acts to reduce the dry bias in the boundary layer. As the radiation scheme is called before the microphysics in the SCM, the radiative properties of the clouds are similar to those from the diagnostic cloud-scheme simulation, although the PC2 simulation produces a larger overestimate of incoming short-wave radiation at the surface (see Figure 2(e)).

The modelled cloud fractions from convective clouds with tops extending to 8 km was shown in Figure 1 to be overestimated in both simulations during the suppressed phase. A lack of mid-level cloud cover is a well known shortcoming of GCMs. In the tropics this error has been associated with a lack of detrainment from the cumulus parametrization at these levels (e.g., Bodas-Salcedo *et al.*, 2008) and the temperature and moisture increments in Figure 7 show that the extensive mid-level clouds in the simulations is forced by the advective tendencies derived from the observations. Even though congestus convection is not explicitly parametrized in the MetUM, Willet *et al.* (2008) showed that the model is capable of producing this type of convection in suppressed regimes, although in their three-dimensional simulations the convection was too weak and shallow compared with cloud resolving model results. In this case study the congestus convection during the suppressed monsoon phase dries the environment too much, particularly in the PC2 simulation (Figure 3).

Similar to the active monsoon phase the strength of convection averaged over the suppressed phase is weaker in the PC2 simulation, except for the heights between 3 and 7 km where the average mass flux is very similar between the two simulations (Figure 5). This average is produced in a different way than during the active phase, with weaker deep convection in the prognostic scheme simulation and larger mass fluxes from mid-level convection in the low to mid-troposphere. During the suppressed monsoon phase the prognostic cloud-scheme simulation produces less

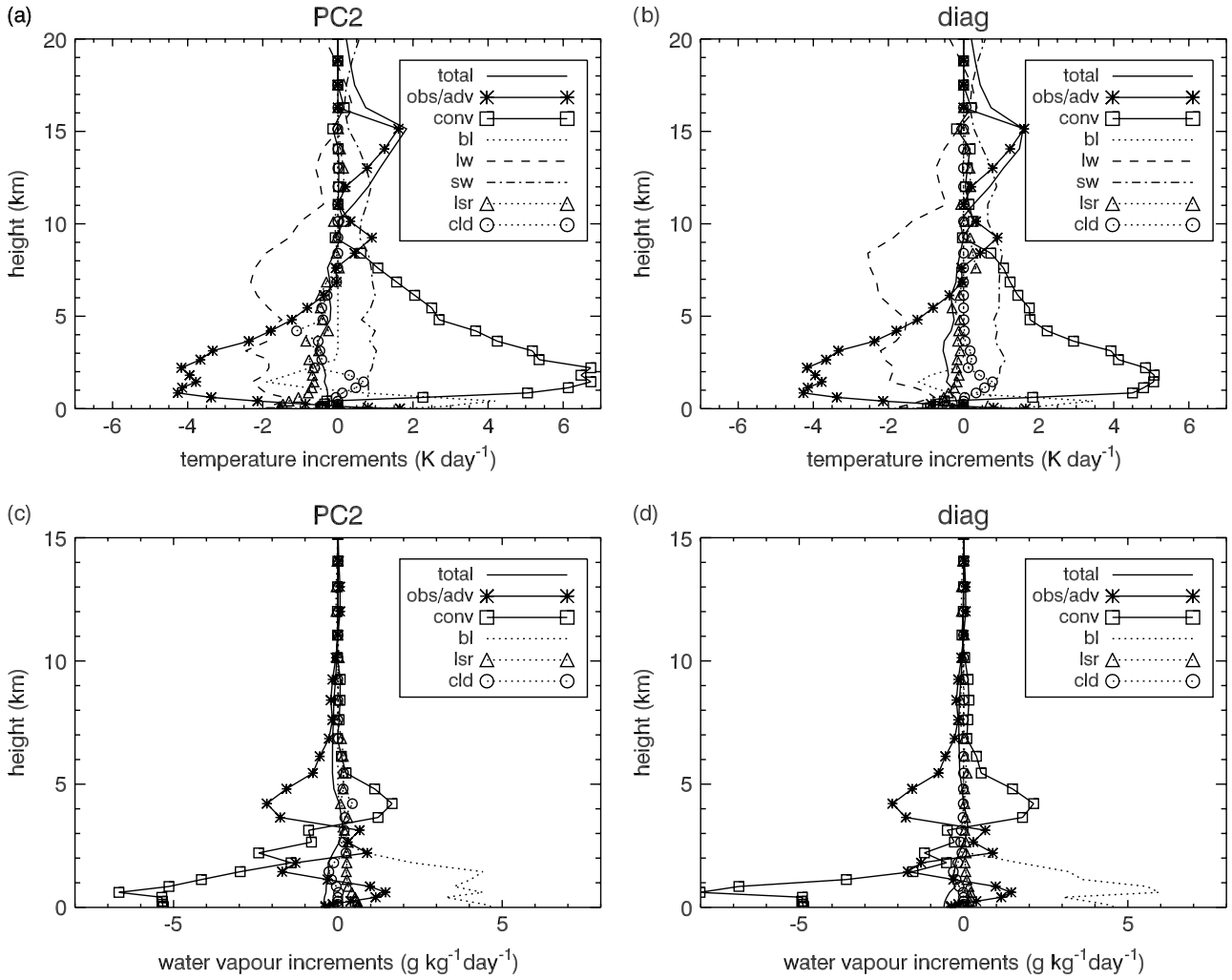

Figure 7. As in Figure 4 except for the suppressed monsoon phase.

detrainment than the diagnostic scheme simulation but a lot more evaporation (Figure 6). However, similar to the active monsoon phase the balance is not achieved in the models, with a larger negative relative humidity bias produced in the PC2 simulation. As discussed in the previous section the reason for the relative humidity differences between the simulations in convective environments is mostly due to the direct detrainment of condensate into the large scale in the prognostic scheme simulation, which as will be shown in section 6 produces an overestimate of the in-cloud ice-water contents of these clouds. The large in-cloud ice-water contents allow large particles to form that quickly fall to the surface and limit the evaporation in the cloud and sub-cloud layers. Note that the tuning applied to the convective precipitation function occurs only deep in the convective plumes (Wilson *et al.*, 2008b) and is not having an effect for these suppressed monsoon phase convective clouds with tops up to 8 km. Typically the convective processes during suppressed convection act to moisten the atmosphere, preconditioning the environment for subsequent deep convection (e.g. Johnson and Lin, 1997). The moisture errors shown by the model parametrizations in the suppressed phase of TWP–ICE will have an impact on the ability of the three-dimensional model to correctly simulate tropical variability.

4. Comparison of cloud variability between the prognostic and diagnostic cloud schemes

The TWP–ICE dataset is one of the most comprehensive datasets to jointly evaluate tropical clouds and the large-scale environment they are embedded in. This section will take advantage of this by developing some diagnostic approaches that aim to provide more insight into the simulation of the cloud fields in the SCM. The two model versions employed here use significantly different treatments of clouds and it is of great interest to highlight possible reasons for the differences in the cloud simulations as well as advantages and disadvantages of the methods employed. One of the most important distinctions between the model versions is the interaction between the convection and the stratiform cloud schemes. In the PC2 simulation the convection scheme detrains condensate and associated cloud fraction, directly into the cloud scheme thereby allowing the prognostic cloud scheme to reflect details of the convective clouds. This differs from the diagnostic scheme where the detrained condensate evaporates and the radiative effect of the convective cloud is represented by a separate diagnostic cloud category. Interesting insight on these scheme interactions can be obtained by comparing the resulting cloud fields for the TWP–ICE case, which exhibits quite varied convection characteristics.

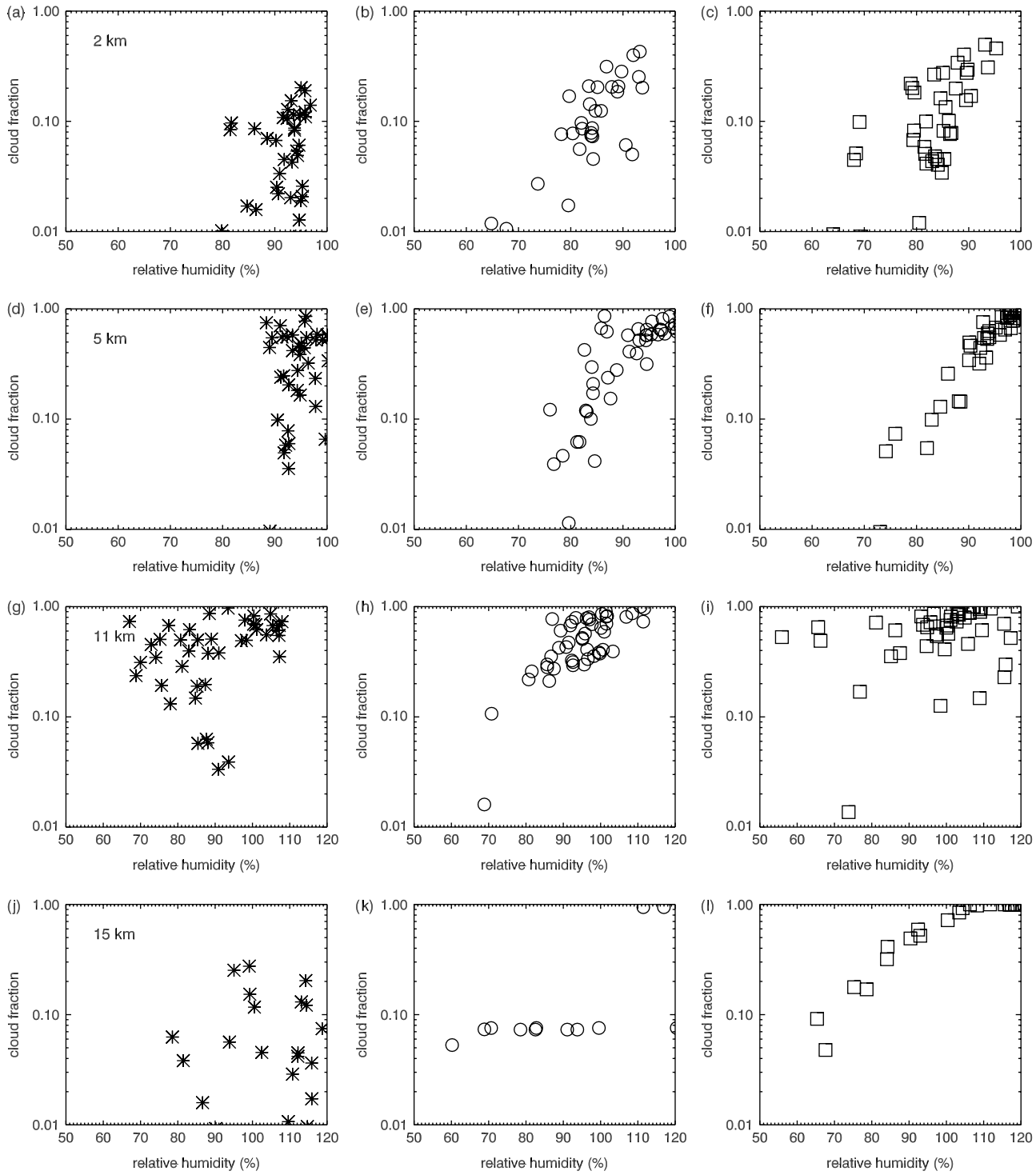

Figure 8. Three-hourly averages of cloud area fraction during the active monsoon phase plotted as a function of relative humidity at the heights of 2, 5, 11 and 15 km for the observations (asterisk: a,d,g,j), the SCM with the prognostic cloud scheme (circle: b,e,h,k) and the SCM with the diagnostic cloud scheme (square: c,f,i,l).

Early cloud parametrizations were frequently based on an explicit relationship between grid-average relative humidity and cloud fraction (e.g., Slingo, 1987). None of the two schemes employed here uses such an explicit relationship and it is therefore of interest to compare the simulated relative humidity–cloud fraction relationships with those from the TWP–ICE dataset. Figure 8 shows the area cloud fractions during the active phase of TWP–ICE, plotted as a function of relative humidity at four different heights. The observed relative humidity has been calculated from the observed/analysis temperature and specific humidity fields using the same equations that are used in the model to calculate the saturation mixing ratio. For temperatures above 0°C vapour saturation pressure over water is used and below this temperature the saturation is calculated over ice. At 2 km all observed clouds during the active monsoon phase of TWP–ICE occur at relative humidities of 80% or higher (Figures 8(a)–(c)). The bulk of the simulated clouds also occur above this relative humidity, however, both simulations produce clouds at significantly

lower relative humidities and in general the model clouds occur at lower relative humidities than the observations. The models produce too many clouds with cloud fractions >0.15. The largest three-hourly averaged cloud fraction observed at 2 km is 0.2, whereas the models both produce cloud fractions >0.4. At 2 km the observations do not show a tendency for higher cloud fractions to be associated with higher relative humidities, however, this relationship is shown in the simulated cloud fields.

Figures 8(d)–(f) show that at 5 km the number of occurrences of clouds with area fraction <0.1 is well captured by the models, however, these clouds are produced when the relative humidity is about 10% less than that observed. There are no observed clouds with a cloud fraction of 1 at this height during the active period, however, the diagnostic scheme produces numerous occurrences of clouds with 100% cloud cover. While the prognostic scheme does not produce total cloud cover at any time, the values from PC2 are typically higher than those observed. As at 2 km, the models show a strong relationship between higher cloud fractions occurring at higher relative humidities, with correlation coefficients of 0.84 and 0.92 for PC2 and the diagnostic scheme respectively. The observations on the other hand show a correlation <0.4 at 5 km.

At 11 km the observed cloud fractions tend to be larger than 0.1, occurring between relative humidities of 65 and 105% (Figure 8(g)–(i)). The diagnostic scheme captures a wider range of the observed variability in this relationship at 11 km due to the contributions to the cloud fraction from both the large-scale cloud scheme and the convective cloud fraction scheme, however, there are too many clouds produced by this simulation at relative humidities >105%. Both simulations overestimate the number of times that there is total cloud cover, however, PC2 is not as prevalent as the diagnostic scheme in simulating cloud fractions of 1, and represents the number of occurrences of cloud fractions <0.5 reasonably well. At 11 and 15 km the observations and model results produce supersaturation with respect to ice. Supersaturations with respect to ice are commonly observed due to the process of ice crystal nucleation not being activated at low supersaturations (e.g. Heymsfield and Miloshevich, 1993). Many models convert supersaturation directly to ice, as is the equivalent treatment for warm-phase microphysics, however, these models tend to produce upper tropospheric dry biases (see e.g. Tompkins *et al.*, 2007).

At 15 km there is only ice cloud and the observations show that the clouds that occur at this height during the active phase occur with cloud fractions <0.3. The diagnostic cloud scheme shows a strong relationship between cloud fraction and relative humidity, something that is not observed nor shown by the prognostic cloud scheme. The clouds at this height represent six separate events in the observations but only two in the PC2 simulation and three in the diagnostic scheme simulation. The first event is at the beginning of the experiment (Figure 1) and the cloud fractions generated by the prognostic scheme sit in the middle of the observations with values of about 0.08 that are independent of relative humidity. The second event for the PC2 simulation is at the end of the active period when a mesoscale convective system developed in the TWP–ICE domain. Both of the simulations produce complete cloud cover for this event at 15 km, with some clouds produced at 120% relative humidity. The observations on the other hand produce cloud fractions for this event of <0.3 at 15 km and the relative humidities at which these clouds occur do not exceed 110%. As discussed previously, the cloud radar was operating with reduced sensitivity during TWP–ICE, however, deriving cloud cover from IR satellite data shows that the high cloud fraction derived from the radar–lidar at these times was underestimated by no more than 10%. Both of the models produce larger and more persistent cloud cover at 15 km than is observed. The positive relative humidity bias that is generated at the tops of convective clouds is part of the reason for the models producing higher and more persistent cloud cover than observed, particularly during the final days of the active period when the strength of convection was overestimated in the simulations.

During the suppressed monsoon phase the observed clouds tend to occur at lower relative humidities than during the active phase (Figure 9). Both models fail to capture the clouds that occur with relative humidities <40% at 2 km. At humidities greater than this the prognostic scheme represents the observed relationship between cloud fraction and relative humidity well, better than the clouds at 2 km during the active monsoon phase. The simulation using the diagnostic cloud scheme, with a separate diagnostic cloud fraction to represent the convective clouds, produces cloud fractions that are generally much larger than those observed at both 2 and 5 km. At 5 km PC2 produces a good representation of cloud fractions, though, as with the diagnostic cloud-scheme simulation, there are more occurrences of cloud at this height than in the observations. These results demonstrate that the prognostic cloud scheme is able to represent cloud cover from both convective and large-scale sources without using a separate scheme as is the case for the diagnostic cloud-scheme simulation.

Figures 9(g)–(i) show that during the suppressed monsoon phase near the base of the cirrus cloud at 11 km the observations and modelled cloud fractions show a strong relationship with relative humidity. Both of the models exhibit a tighter relationship than is observed and produce more occurrences of cloud fractions larger than 0.2 and not enough <0.1. Similarly at 15 km neither of the models simulate the numerous observed cloud fractions <0.1 and produce many instances of three-hourly averaged total cloud cover that is never observed. It is worth noting that if the observed horizontal advection of cloud fraction was available and included in the forcing, this would act to further increase the PC2 cloud fraction in the upper levels. As in the active monsoon phase at 15 km there are times when PC2 generates ice cloud fractions that are independent of relative humidity as shown in Figure 9(k), and also apparent at 11 km in Figure 9(h). These instances occur when cloud fraction generated at this height remains at constant values for extensive periods of time and shows no sensitivity to the relative humidity fluctuations of the environment. The reason for this is the assumptions relating to which microphysical processes cause a change in the prognostic cloud fractions. In PC2 ice cloud fraction reduces due to the microphysical processes of sublimation, melting and evaporation, with the fall of ice increasing the cloud fraction when the cloud fraction of the layer above is greater than that in the present layer (Wilson *et al.*, 2008a). The process of deposition is assumed to increase the ice water content (IWC) but not the cloud fraction. In the long-lived cirrus cloud of the suppressed monsoon phase, the upper levels of the cloud act as the generating layer, with depositional growth and fall out of ice the only microphysical

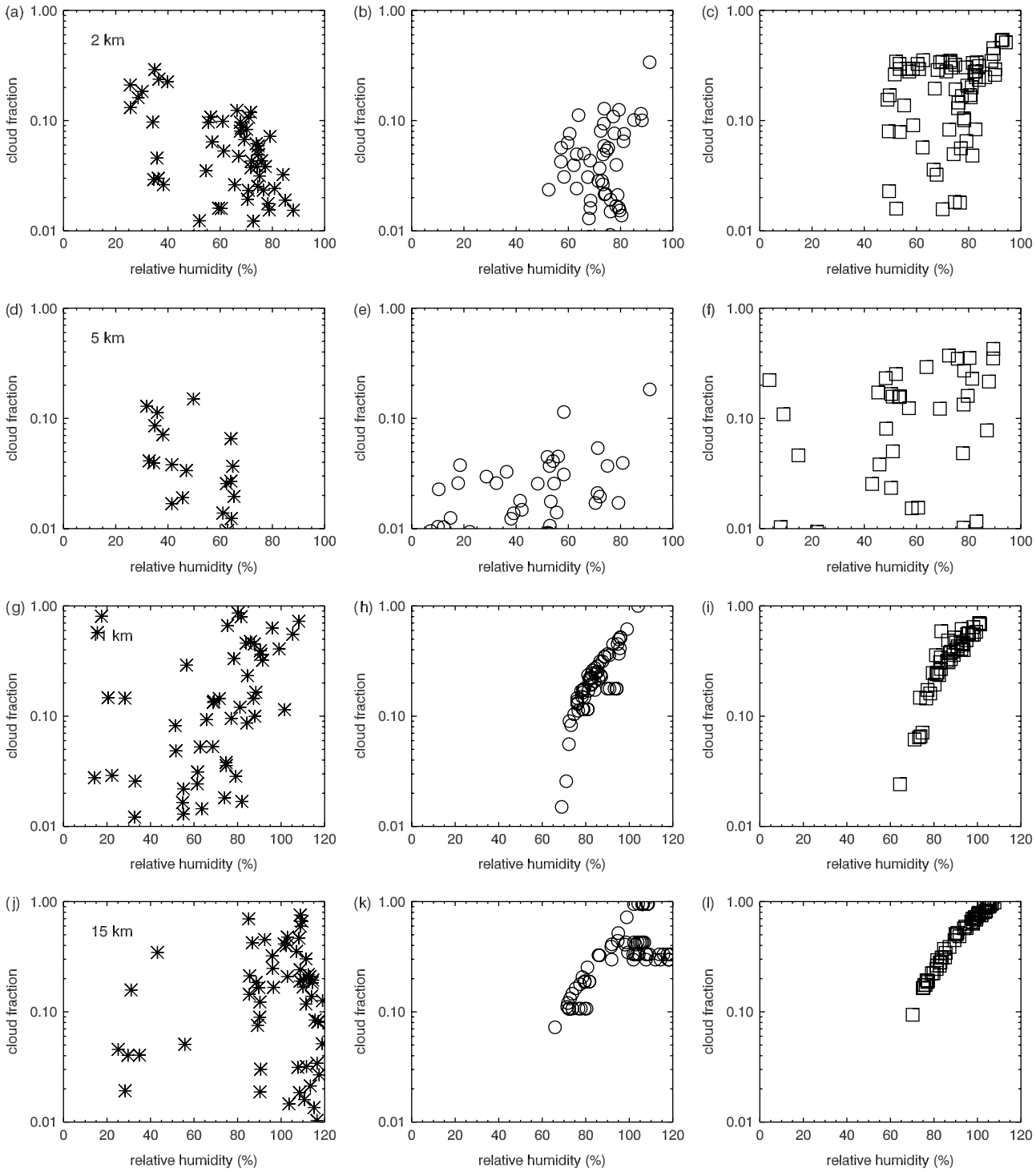

Figure 9. As in Figure 8 except for the suppressed monsoon phase.

processes active in the model. While the ice-water content fluctuates due to these processes, the cloud fraction does not. The constant value of the PC2 cloud fraction during these times generally agrees better with the observations than the diagnostic scheme in these cloud layers, however, there is no correlation between the changes in IWC and cloud fraction in the PC2 simulation. The observations at the top of the cirrus cloud have a correlation coefficient between IWC and cloud fraction of 0.85, the corresponding value for the diagnostic scheme is 0.72, while for PC2 the value is −0.1. Lower in this cloud layer sublimation occurs and consequently reduces the PC2 ice cloud fraction as a function of the reduced ice-water content and produces correlation coefficients of 0.84 for PC2, 0.8 for the diagnostic scheme and 0.78 for the observations.

Using the same assumptions that are made in PC2 for the effect of sublimation on the cloud fraction (Wilson *et al.*, 2008a), the effect of depositional growth on the ice cloud fraction can be formulated as

$$\Delta C_i = A\left(1 + \frac{\Delta\overline{qi}}{\overline{qi}(A/C_i)}\right)^{1/2} - A \qquad (1)$$

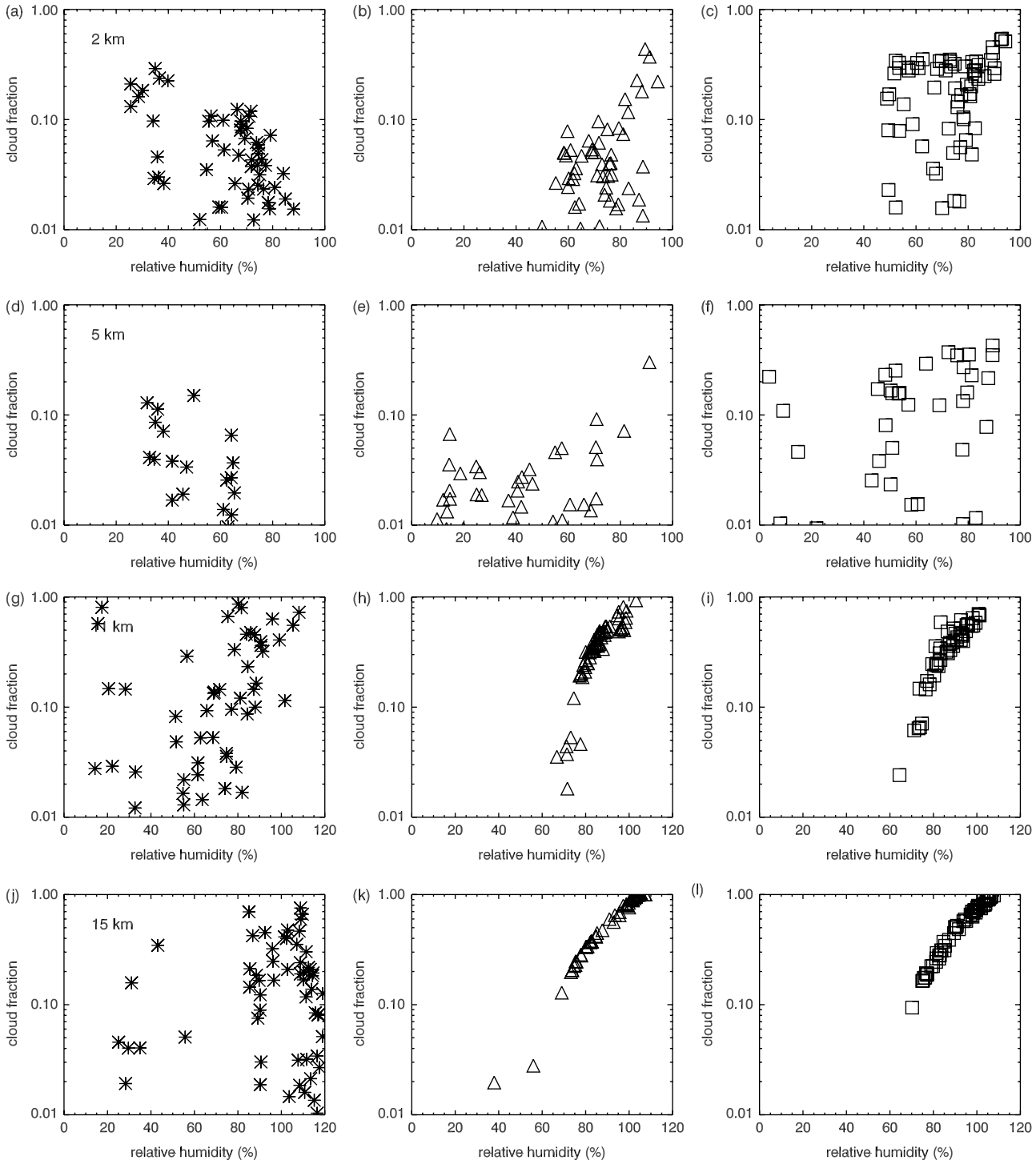

Figure 10. As in Figure 9 except that it shows the PC2 cloud fractions that are simulated when the effect of depositional growth of ice particles is included as a source of cloud fraction (triangle).

where C_i is the ice cloud fraction, A is the area of the grid box that contains ice and is above ice saturation, $\overline{qi}$ is the grid box mean ice water and $\overline{qi}(A/C_i)$ is the amount of ice that is present in the region of the grid box where deposition is occurring. Allowing the cloud fraction to increase as a function of the vapour depositional growth rate of ice gives more realistic variations in the PC2 cloud fractions (see Figure 10). The result of deposition acting as a source of ice cloud fraction produces cloud cover that more closely resembles that from the Smith scheme at 15 km, with the cloud fractions now converging to total cloud cover as the relative humidity approaches 100%. This change to PC2 results in larger cloud fractions in the upper troposphere and while many aspects of the TWP–ICE simulation are improved with this change, other biases, such as the too low OLR during the early morning hours, are exacerbated. Further work is currently underway to examine the effects of additional microphysical source and sink terms on the cloud fractions, although the preliminary results presented in Figure 10 look promising and the inclusion of the deposition term as a source of cloud fraction improves ACCESS coupled model simulations (Zhian Sun, 2011; personal communication).

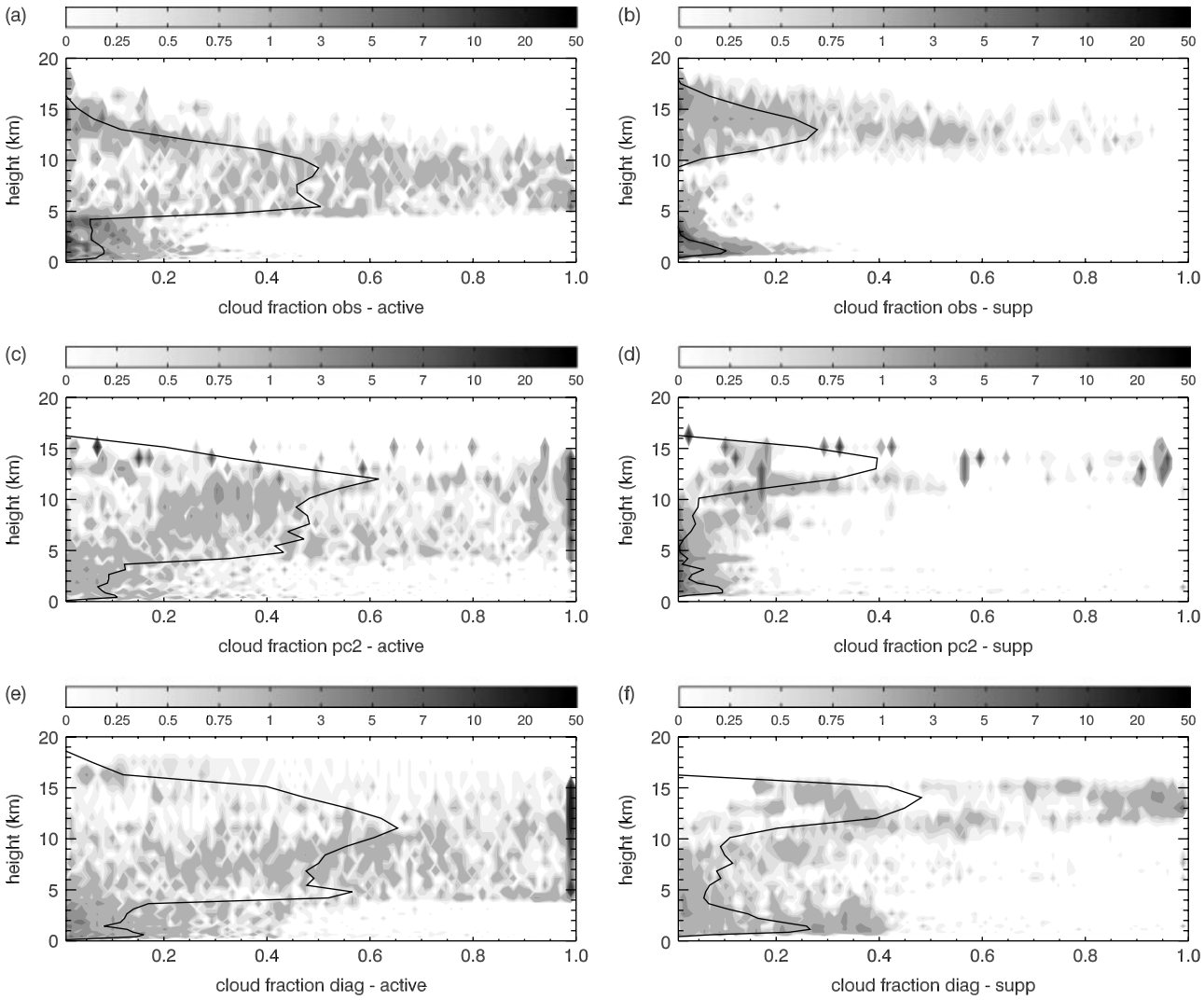

Figure 11. (a) Normalized histogram of the observed cloud area fraction as a function of height during the active monsoon phase with the solid line showing the average cloud fraction. (c) As for (a) except for the SCM results for the PC2 scheme. (e) As for (a) except for the SCM results for the diagnostic cloud scheme. (b), (d) and (f) As in (a), (c) and (e) except for the suppressed monsoon phase.

The vertical distribution of clouds, along with the total cloud amount and optical properties, determines the radiative budget of the atmospheric column. The observations of the average cloud vertical distribution at the main ARM site in Darwin (Figure 11(a)) show a trimodal structure during the active phase with peaks at 1, 5.5 and 9.5 km, similar to other studies of tropical convection (Johnson *et al.*, 1998). The lowest peak is from shallow boundary layer clouds, the middle peak is due to the low to mid-level clouds occurring during the earlier stages of the monsoon convective systems lifecycle (Xie *et al.*, 2010) and the highest peak is from anvil clouds developed from the outflow of deep convection. The SCM vertical cloud distributions have average peaks at similar heights to the observations, however, the mid- and upper peaks occur at higher altitudes in the models, particularly the upper level peak in PC2, which is 2 km higher than that observed. As well as the average vertical cloud profile, Figure 11 shows normalized histograms of the cloud fraction as a function of height. The observations (Figure 11(a)) show that the boundary layer clouds predominately occur with cloud fractions <0.3. The PC2 cloud scheme produces a good average boundary layer cloud fraction during the active phase, however, there are more clouds simulated with cloud fractions between 0.3 and 0.4 and not enough with fractions of 0.1 and below. The SCM run with the diagnostic cloud scheme shows higher average boundary layer cloud cover than the observations and the PC2 results, predominately due to more occurrences of cloud with cloud fractions >0.25.

When the models simulate cloud between 5 and 10 km during the active phase the cloud fraction tends to be too large (Figures 11(a), (c) and (e)). The observed distribution of cloud cover shows many clouds occurring with cloud fraction between 0.4 and 0.8, however, the PC2 cloud cover for these heights tends to be either close to 1 or <0.4 and overall gives an average smaller cloud fraction. In contrast, the diagnostic scheme produces an average cloud fraction at these heights that is larger than that observed. There is less clear sky in the levels between 8 and 15 km in the models than is observed, particularly the diagnostic scheme that produces frequent occurrences of complete cloud cover. In the levels above 10 km the observations never show cloud fractions of 1, and instead show a tendency to reduce the cloud fraction with height so that at 15 km cloud predominately occurs with cloud fractions <0.1. The prognostic cloud scheme does a better job than the diagnostic scheme at producing the observed normalized histogram in the levels

above 10 km, but still produces too many clouds with cloud fractions larger than 0.95 and as such the average cloud fraction across these levels is higher than that observed.

For the suppressed monsoon phase of TWP–ICE the average observed cloud fraction shows two peaks at 1 and 13 km (Figure 11(b)). There is little observed cloud between 3 and 9 km, with the cloud occurring almost always having cloud fractions <0.1. The average boundary layer cloud cover is captured well with the prognostic cloud scheme but significantly overestimated by the diagnostic scheme. The cloud fraction produced by the diagnostic cloud-scheme simulation in the levels between 3 and 9 km is overestimated, with numerous occurrences of cloud fractions >0.2. The PC2 simulation also overestimates the average cloud cover at these heights, however, the clouds that are produced tend to have cloud fractions <0.1.

The observations show an increase in the height of the high cloud maximum between the active and suppressed phases of about 3.5 km. The height of the PC2 high cloud maximum also increases between the monsoon phases but only by 1 km, which means the height of the maximum is overestimated by 1 km during the suppressed monsoon times. The diagnostic scheme produces the peak high cloud cover at 14 km, the same height as the prognostic scheme, however, the average amount from this simulation is greater than the PC2 cloud fraction and the observations. This is due to the diagnostic scheme producing high cloud with fractions typically larger than 0.85 or between 0.25 and 0.35. As in the active phase the observations show the cloud fraction tends to decrease with height and above 10 km the observed clouds mostly occur with cloud fractions <0.25 during the suppressed phase. The prognostic scheme generates cloud fractions above 10 km with low cloud fractions between 0.1 and 0.25, but also produces cloud fractions of 0.6 and larger more often than is observed. There is almost no observed high cloud during the suppressed monsoon phase with cloud fractions >0.9, whereas, the models simulate a significant number of clouds with these high cloud fractions. The cirrus cloud also extends to 18 km in the observations but due to the lack of forcing above 16 km the models only produce cloud condensate up to this height, as discussed previously.

5. Ice cloud properties during days 25–30 of the suppressed monsoon phase

Observations of IWC and ice fall velocity have been obtained from a radar–lidar retrieval (Delanoë and Hogan, 2008; Protat *et al.*, 2010) for days 25–30 of the suppressed

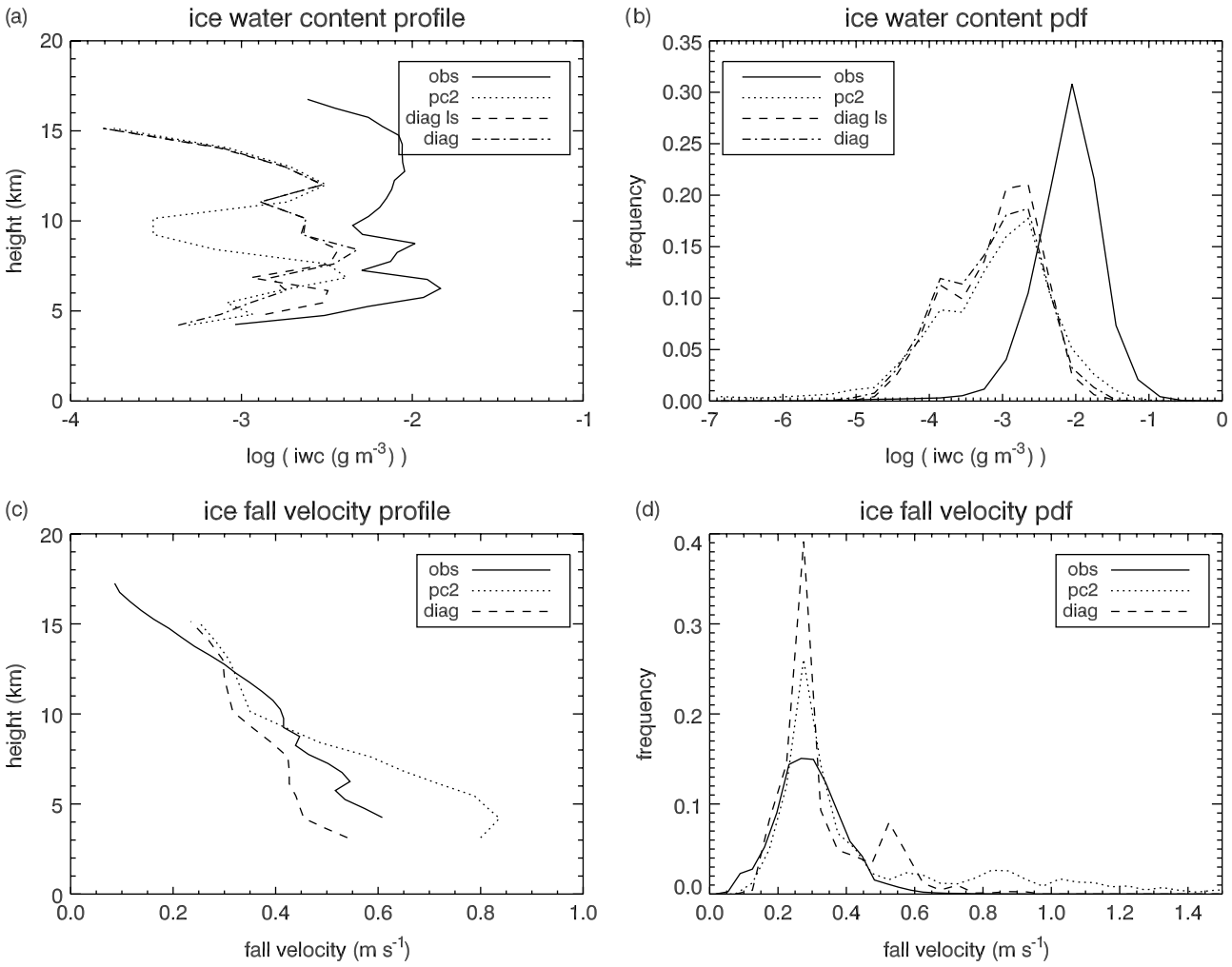

Figure 12. (a) Average profiles of non-zero ice water content (log (g m^{-3})) over days 25–30 for the observations (solid line), the simulation with the PC2 scheme (dashed line), the large-scale component from the simulation with the diagnostic cloud scheme (dotted line) and the convective + large-scale components from the diagnostic scheme simulation (dot-dash line). (b) Probability distribution function of ice water content. (c) Average profiles of ice-fall velocity. (d) Probability distribution function of ice-fall velocity profile. The diagnostic scheme results in (c) and (d) include only the large-scale component.

monsoon phase. Figure 12(a) shows that when ice is present over this 5 day period, the models systematically underestimate the amount observed; note that the ice content is a prognostic variable in both simulations. The observations show a trimodal structure in the ice-water content profile with peaks at 6, 9 and 13 km. The large-scale component of IWC from the diagnostic scheme simulation also shows three peaks at approximately the correct heights, however, the amounts averaged over the times when ice is present are significantly underestimated. When the convective component of ice water is added to the large-scale value the diagnostic scheme simulation produces a result that more closely resembles that from the prognostic scheme in the levels below 6 km. However, care needs to be taken in the interpretation of this comparison below 10 km as the number of occurrences is only four in the observational dataset and at these times there was precipitation reaching the surface, which can cause attenuation and as such uncertainties in the quantities retrieved.

Both simulations produce a peak in IWC at 12 km, however, the cloud ice-water contents from PC2 below 11 km drop off by more than an order of magnitude compared with small changes from the diagnostic scheme simulation. The PC2 simulation produces an average non-zero value at 10 km of 2.8×10^{-4} g m^{-3} (the threshold used in the calculations is 1×10^{-10} g m^{-3}), which is significantly less than the observed value of 4×10^{-3} g m^{-3}. At 10 km the cumulative ice-water contents over this 5 day period agree well between the observations and the two model results (not shown), even though as Figure 12(a) shows this agreement comes about due to large differences between the modelled amounts and hence number of occurrences. The distribution of IWC over these 5 days illustrated in Figure 12(b) shows that the prognostic scheme produces more variability in ice amounts, however, both simulations underestimate the amount seen in the observations, with PC2 producing more occurrences of high ice-water content than the diagnostic scheme simulation. The observed distribution in Figure 12(b) agrees well with the observations over Darwin presented in Protat *et al.* (2010) that covered a 6 month period.

The particle size distributions used in the model and IWC retrieval are both based on gamma functions, although they do differ in their formulations and this may lead to some differences between the models and observations. However, as shown in an objective intercomparison study by Heymsfield *et al.* (2008), the size distribution assumption used for the IWC retrieval is not typically the main source of error. The underestimate of modelled IWC found for TWP–ICE agrees with the underestimate of IWC in frontal clouds in the MetUM that was documented by Bodas-Salcedo *et al.* (2008) using CloudSat radar reflectivities. In that case the microphysical assumptions, including the size distributions, were made as consistent as possible between the model and the observations.

The average fall velocity of ice decreases as the height at which it occurs increases in both the model and the observations, as shown in Figure 12(c). The diagnostic cloud scheme produces a gradient of this change in fall speed with height closest to the observations in the levels below 8 km, however, the average values are slower than the observations, while those from PC2 are faster. Figures 12(c) and (d) show only the ice-fall velocities for the large-scale component of ice water from the diagnostic scheme simulation because the microphysics in the convection scheme is highly simplified in the model and does not allow for the calculation of a fall speed. Given that the in-cloud IWCs from the diagnostic scheme simulation cover a similar range of values when the convective component is excluded (not shown), the fall speeds shown in Figures 12(c) and (d) would not be expected to vary greatly if we included the convective cloud values.

The observations have been converted from a reflectivity-weighted fall speed to a mass-weighted fall speed so as to match the model results. The conversion applied assumes that the reflectivity-weighted value is 1.4 times the mass-weighted fall speed, however, there will be some variability in this linear conversion based on the properties of the ice clouds changing with height (Matrosov and Heymsfield, 2000). The faster fall speed from the prognostic cloud scheme compared with the diagnostic scheme reflects the increase in the amount of in-cloud IWC in the levels below 8 km in the PC2 simulation (Figure 13). Above 12 km the models produce faster fall speeds than the observations, even though the IWC at these heights is significantly less than that observed (see Figure 12(a)). This implies that the observations have smaller sized particles in larger concentrations than the models and could be caused by any number of deficiencies in the model parameterizations, including the assumed ice particle size distribution, the fall speed equation, and the formulations for growth of particles by deposition and aggregation.

The majority of the ice falls with velocities between 25 and 30 cm s^{-1} in both the models and the observations (Figure 12(d)), however, the models both show larger skewness and kurtosis in their distributions of ice-fall velocity. The peak of the distribution being well represented by the models gives further support for the size distribution differences between the models and the retrieval not contributing significantly to the disagreement shown in Figure 12(c). The distribution from the simulation with the diagnostic cloud scheme is bimodal with a secondary peak at 50–55 cm s^{-1}, which is not seen in the observations. The PC2 distribution of ice-fall speeds is more representative of the observations than the diagnostic scheme in terms of the kurtosis, however, the results from this simulation show that the model is at times producing fall speeds that are much larger than those observed, with the maximum fall speed simulated by the prognostic scheme about twice that observed.

The quantity that is important for the microphysical and radiative transfer calculation is the in-cloud condensate, which is the grid-box average condensate amount normalized by the cloud cover. Figure 13 shows the in-cloud IWC plotted as a function of cloud fraction for the observations taken from days 25 to 30 of the suppressed monsoon period and the models at four different heights. At 5 km the diagnostic scheme simulation produces too many occurrences of large in-cloud IWC compared with the observations and these tend to occur with much larger associated cloud fractions. The prognostic cloud scheme produces significantly more occurrences of high in-cloud IWC at 5 km compared with both the observations and the diagnostic scheme simulation, however, in contrast to the diagnostic scheme results the associated cloud fractions are <0.05, which is the value that the observed cloud fractions tend to be at this height (Figure 13(a)–(c)). These high values of in-cloud IWC allow the growth of large particles in the PC2 simulation and are the reason why the fall speeds at this height are faster than

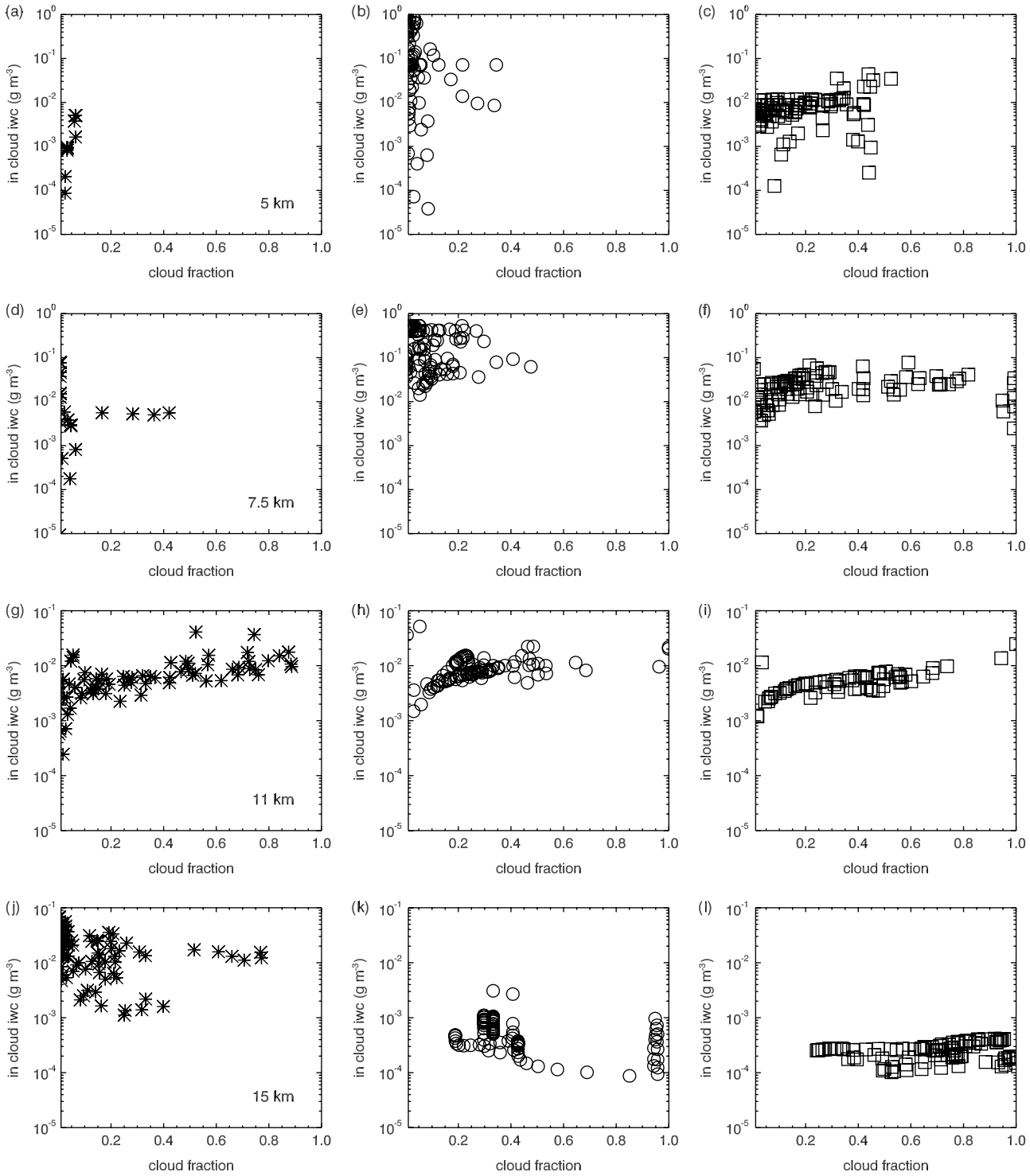

Figure 13. In-cloud ice water content (IWC/cloud fraction) (g m^{-3}) over Julian days 25–30 plotted as a function of cloud fraction at the heights of 5, 7.5, 11 and 15 km for the observations (asterisk: a,d,g,j), the SCM with the prognostic cloud scheme (circle: b,e,h,k) and the SCM with the diagnostic cloud scheme, where the ice water content includes the contribution from both convective and large-scale sources (square: c,f,i,l). At 11 and 15 km every third data point is plotted.

those observed (see Figure 12(c)). The PC2 simulation produces higher in-cloud IWC compared with the observations, typically by two orders of magnitude. A similar result can be seen at 7.5 km with both simulations overestimating the in-cloud IWC, more so for the prognostic cloud-scheme simulation (Figure 13(d)–(f)).

The in-cloud IWC at 11 km is well simulated by both models (Figure 13(g)–(i)), with the observed tendency for in-cloud IWC to decrease with decreasing cloud fraction captured by both cloud schemes. The diagnostic scheme results tend to underestimate the in-cloud IWC, while on average PC2 captures the observed values. At 15 km the models and the observations sit in different phase spaces. The observations show typical in-cloud IWCs of between 0.1 and 0.01 g m^{-3}, whereas the models are both generally two orders of magnitude less, with PC2 typically generating higher in-cloud IWCs than the simulation with the diagnostic cloud scheme. The models produce cloud fractions at this

height that are too large (Figure 13(j)–(l)), and this result, compounded with the much smaller IWCs that the models produce at 15 km (Figure 12(a)), is the reason why the models have significantly smaller in-cloud IWCs. The large-scale ice cloud fraction in the diagnostic cloud scheme increases as a monotonic function of increasing IWC, and the observations at 15 km do not show this relationship. This highlights the need for a prognostic cloud scheme to be able to obtain the observed relationship between ice cloud fraction and IWC.

Using observations from three field campaigns consisting mostly of stratocumulus and frontal cirrus, Wood and Field (2000) showed that the Smith scheme tends to underpredict cloud fraction for a given grid-box mean condensate. However, for the case of the cirrus cloud during the suppressed monsoon phase of TWP–ICE, if the observed values of IWC, temperature and water vapour are used to calculate the cloud fraction from the Smith scheme, the result is an overestimate of cloud cover. Therefore, even if the model produced unbiased temperature, moisture and IWCs, the cloud fraction for this cloud would still be too large.

6. Summary and discussion

The ACCESS SCM, which is equivalent to the MetUM SCM of the UK Met Office, has been used to simulate the TWP–ICE period to investigate the ability of the model to represent the vertical distribution and temporal evolution of tropical cloud systems. Two SCM simulations have been analysed, each using a different representation of clouds. A new prognostic cloud scheme, PC2, has been developed at the UK Met Office to overcome some of the problems associated with the tightly constrained cloud fields that are produced by the diagnostic scheme used in the MetUM. The ACCESS SCM produced generally reasonable representations of the TWP–ICE cloud fields. Both simulations overestimate the average high cloud cover, however, this is due to different distributions of cloud cover from the two cloud schemes. While the diagnostic scheme tends to predominately produce cloud fractions close to 1, PC2 produces less overcast conditions with more occurrences of low cloud fractions, in better agreement with the observations. However, the total column cloud cover from the prognostic cloud scheme is significantly underestimated. The observations show a tendency during both the active and suppressed monsoon phases to reduce the cloud cover as a function of height in the upper troposphere. Both cloud scheme simulations show a weaker tendency for this trend during the active phase of TWP–ICE, however, only the prognostic scheme shows any evidence of this trend during the suppressed phase. The average low-level cloud cover from the prognostic cloud scheme agrees reasonably well with the observations during both monsoon phases, whereas the low cloud cover from the diagnostic scheme simulation is too large.

The direct detrainment of condensate and cloud fraction from convection into the large-scale variables in the prognostic cloud-scheme simulation changes the moistening due to convective detrainment and large-scale evaporation compared with the diagnostic-cloud scheme simulation. This results in a larger negative relative humidity bias for the prognostic cloud-scheme simulation in the mid-lower troposphere, particularly during the suppressed monsoon phase. The drier atmosphere reduces the average updraft mass flux in the PC2 simulation, however, during the active monsoon phase when the deep convection scheme in the model is triggered, the associated convection is stronger in the prognostic scheme simulation and there is less mass flux produced by mid-level convection. During the suppressed monsoon phase the prognostic cloud-scheme simulation produces large values of in-cloud IWC that are significantly greater than the observations and the diagnostic scheme simulation in the levels below 8 km. This allows the growth of large particles with faster fall speeds than observed, that rapidly fall to the surface limiting the evaporation in the cloud and sub-cloud layers.

In a study of climate sensitivity using a multithousand member ensemble Sanderson *et al.* (2008) found that the two parameters that explained 70% of the variance were the ice-fall speed and the entrainment coefficient. This result suggests that in order to reduce uncertainty in climate projections greater accuracy in the representations of the ice-fall speed are necessary, which implies that the ice properties in models, including the size distributions, need to be better constrained. For the initial suppressed phase of TWP–ICE the models produced faster ice-fall speeds in the upper troposphere, which together with an underestimate of the IWC means that the observations have smaller sized particles in larger concentrations than the models. The model does not assume that supersaturation with respect to ice in a cloudy portion of the grid box is immediately converted to ice and instead explicitly models the process of deposition, therefore, the microphysical processes and the distribution of moisture are important in determining the IWC from large-scale processes. The faster fall speeds at the top of the cloud will reduce the time that the particles have to grow within these cloud layers, which will contribute to the underestimate of IWC shown. As well as the size distribution and formulation of the microphysical processes, the subgrid-scale moisture distribution in the model strongly influences the amount of moisture available for the growth of ice particles (Wilson *et al.*, 2008a). This distribution in the MetUM creates a subgrid horizontal water flux that enhances the moisture in the cloudy part of the grid box at the expense of the clear-sky moisture (Tompkins *et al.*, 2007), yet the IWCs are underestimated in this case study. The moisture distribution that influences the IWC is a function of a number of tuning parameters: the critical relative humidity and the width of the moisture distribution in the portion of the grid box that contains ice (Wilson and Bushell, 2007). All of these parametrizations and parameters affect the IWC produced by the model and further research is needed to determine the key sources of the error.

One of the disadvantages of a scheme with prognostic cloud fractions is the complexity due to the need to represent source and sink terms for each physical process in the model. A long-lived cirrus cloud during the suppressed monsoon phase showed that the assumptions in PC2 that depositional growth and fall out of ice do not change the cloud fractions resulted in constant cloud fractions for close to 2 days. The addition of depositional growth as a source of ice cloud fraction in PC2 produced cloud fractions above 10 km that agree more with those from the diagnostic cloud scheme and reduced the underestimate in total column cloud fraction and on average improved the radiative fluxes.

Lin *et al.* (2004) suggested that the inability of many models to simulate realistic representations of the

Madden–Julian oscillation (MJO) may be caused by systematic diabatic heating profile errors. Temperature and moisture errors in the SCM simulations were seen to be the most pronounced during the suppressed monsoon period and also quite different between the two simulations. This suggests that the choice of cloud scheme and the way that the scheme interacts with the convection scheme plays an important role in the relative humidity errors during times of suppressed convection. Other studies such as Li *et al.* (2008) have identified the link between poor simulations of suppressed convection leading to unrealistic simulations of subseasonal variability in tropical convection, including the MJO. The GEWEX Cloud Systems Study Group (GCSS) is currently organizing a model intercomparison study based on TWP–ICE. The experiments being performed use the forcing and evaluation dataset that was used in this study. Hence, the outcomes of these model simulations, in particular the high resolution CRMs, will enable a more rigorous assessment of the link between the cloud scheme and the convection parametrization in the ACCESS/MetUM SCM.

Acknowledgements

This work was supported by the Australian Climate Change Science Program. Christian Jakob is grateful for support from the US Department of Energy under grant DE-FG02-03ER63533 as part of the Atmospheric Radiation Measurement Program. Data were obtained from the Atmospheric Radiation Measurement (ARM) Program sponsored by the US Department of Energy, Office of Science, Office of Biological and Environmental Research, Environmental Sciences Division. The radar–lidar retrievals used in this study were generated by Julien Delanoë from the University of Reading and the cloud-top temperature data were processed by Michael Whimpey from CAWCR. CNF would like to acknowledge Drs Damian Wilson and Jon Petch from the Met Office for discussions and insight on PC2. Drs Peter May, Zhian Sun and Leon Rotstayn (CAWCR) are thanked for providing helpful comments on the manuscript, as are two anonymous reviewers whose comments improved the manuscript.

References

Bergman JW, Sardeshmukh PD. 2003. Usefulness of single column model diagnosis through short-term predictions. *J. Climate*, **16**: 3803–3819.

Bodas-Salcedo A, Webb MJ, Brooks ME, Ringer MA, Williams KD, Milton SF, Wilson DR. 2008. Evaluating cloud systems in the Met Office global forecast model using simulated CloudSat radar reflectivities. *J. Geophys. Res.* **113**: DOI:10.1029/2007JD009620.

Boyle J, Klein SA. 2010. Impact of horizontal resolution on climate model forecasts of tropical precipitation and diabatic heating for the TWP–ICE period. *J. Geophys. Res.* **115**: DOI:10.1029/2010JD014262.

Chen SS, Houze RA Jr. 1997. Diurnal variation and life-cycle of deep convective systems over the tropical Pacific warm pool. *Q. J. R. Meteorol. Soc.* **123**: 357–388.

Clothiaux EE, Ackerman TP, Mace GG, Moran KP, Marchand RT, Miller MA, Martner BE. 2000. Objective determination of cloud heights and radar reflectivities using a combination of active remote sensors at the ARM CART sites. *J. Appl. Meteor.* **39**: 645–665.

Collins W, Bellouin N, Doutriaux-Boucher M, Hinton T, Jones CD, Fiddicoat S, Martin G, O'Connor F, Rae J, Reddy S, Senior C, Totterdell I Woodard S. 2008. *Evaluation of the HadGEM2-ES model.* Hadley Centre Technical Note 74, 43 pp. http://www.metoffice.gov.uk/research/hadleycentre/pubs/HCTN/index.html

Delanoë J, Hogan R. 2008. A variational scheme for retrieving ice cloud properties from combined radar, lidar and infrared radiometer. *J. Geophys. Res.* **113**: D07204, DOI:10.1029/2007JD009000.

Derbyshire SH, Beau I, Bechtold P, Grandpeix J-Y, Piriou JM, Redelsperger J-L, Soares PM.M. 2004. Sensitivity of moist convection to environmental humidity. *Q. J. R. Meteorol. Soc.* **130**: 3055–3079.

Ghan SJ, Leung LR, McCaa J. 1999. A comparison of three different modelling strategies for evaluating cloud and radiation parameterizations. *Mon. Wea. Rev.*, **127**: 1967–1984.

Gregory J. 1999. *Representation of the Radiative Effects of Convective Anvils. Hadley Centre Technical Note* 7, Met. Office: Exeter, UK.

Heymsfield AJ, Miloshevich LM. 1993. Homogeneous ice nucleation and supercooled liquid water in orographic wave clouds. *J. Atmos. Sci.* **5**: , 2335–2353.

Heymsfield AJ, Protat A, Austin RT, Bounoil D, Hogan RJ, Delanoe J, Okamoto H, Sato K, van Zadelhoff G-J, Donovan DP, Wang Z 2008. Testing IWC retrieval methods using radar and ancillary measurements with in situ data. *J. App. Meteorol Clim.* **47**: 135–163.

Hume T 2007. Radiation dry bias in the TWP_ICE radiosonde soundings. *The 17th ARM Science Team Meeting*, California, USA. Available from http://www.arm.gov/publications/proceedings/conf17/index.php

Johnson RH, Lin X. 1997. Episodic trade-wind regimes over the Western Pacific warm pool. *J. Atmos. Sci.* **54**: 2020–2034.

Johnson R H, Rickenbach TM, Rutledge SA, Ciesielski PE. Shubert WH. 1998. Trimodal characteristics of tropical convection. *J. Climate* **12**: 2397–2418.

Keenan TD, Carbone RE. 1992. A preliminary morphology of precipitation systems in tropical northern Australia. *Q. J. R. Meteorol. Soc.* **118**: 283–326.

Keenan TD, Glasson K, Cummings F, Bird TS, Keeler, J, Lutz J. 1998. The BMRC/NCAR C-band polarimetric (C-Pol) radar system. *J. Atmos. Oceanic Technol.* **15**: 871–886.

Li C, Jia X, Ling J, Zhou, W, Zhang C. 2008. Sensitivity of MJO simulations to diabatic heating profiles. *Clim. Dynam.* DOI:10.1007/s00382-008-0455-x.

Lin J-L, Mapes B, Zhang, M, Newman M. 2004. Stratiform precipitation, vertical heating profiles and the Madden–Julian oscillation. *J. Atmos. Sci.* **61**: 296–309.

Matrosov S, Heymsfield A. 2000. Use of Doppler radar to assess ice cloud particle fall velocity-size relations for remote sensing and climate studies. *J. Geophys. Res.* **105**: DOI:10.1029/2000JD900353.

May PT, Mather JH, Vaughan G, Jakob CN, McFarquhar GM, Bower KN, Mace GG. 2008. The Tropical Warm Pool International Cloud Experiment (TWP–ICE). *Bull. Am. Meteorol. Soc.* **89**: 629–645.

Menon S, Brenguier J-L, Boucher O, Davison P, Del Genio AD, Feichter J, Ghan S, Guibert S, Liu X, Lohmann U, Pawlowska H, Penner JE, Quaas J, Roberts DL, Schüller, L, Snider J. 2003. Evaluating aerosol/cloud/radiation process parameterizations with single-column models and Second Aerosol Characterization Experiment (ACE-2) cloudy column observations. *J. Geophys. Res.* **108**: DOI:10.1029/2003JD003902.

Petch JC. Willett M, Wong RY, Woolnough SJ. 2007. Modelling suppressed and active convection. Comparing a numerical weather prediction, cloud-resolving and single-column model. *Q. J. R. Meteorol. Soc.* **133**: 1087–1100.

Protat A, Delanoë J, Plana-Fattori A, May PT, O'Connor E. 2010. The statistical properties of tropical ice clouds generated by the West-African and Australian monsoons from ground-based radar-lidar observations. *Q. J. R. Meteorol. Soc.* **136**(S1): 345–363, DOI: 10.1002/qj.490.

Randall DA, Xu K-M, Somerville RJC, Iacobellis S. 1996. Single-column models and cloud ensemble models as links between observations and climate models. *J. Climate* **9**: 1683–1697.

Sanderson BM, Piani C, Ingram WJ, Stone DA. Allen MR. 2008. Towards constraining climate sensitivity by linear analysis of feedback patterns in thousands of perturbed-physics GCM simulations. *Clim. Dyn.* **30**: 175–190.

Smith RN.B. 1990. A scheme for predicting layer clouds and their water contents in a general circulation model. *Q. J. R. Meteorol. Soc.* **116**: 435–460.

Slingo JM. 1987. The development and verification of a cloud prediction model for the ECMWF model. *Q. J. R. Meteorol. Soc.* **113**: 899–927.

Tompkins AM, Gierens, K, Rädel G. 2007. Ice supersaturation in the ECMWF integrated forecast system. *Q. J. R. Meteorol. Soc.* **133**: 53–63.

Willett MR, Bechtold P, Williamson DL, Petch JC, Milton SF, Woolnough SJ. 2008. Modelling suppressed and active convection: Comparisons between three global atmospheric models. *Q. J. R. Meteorol. Soc.* **134**: 1881–1896.

Wilson, D, Bushell A. 2007. *Annexe to Unified Model Documentation paper 29. The PC2 Cloud Ccheme*. Met Office: Exeter, UK.

Wilson D, Smith RNB, Gregory D, Wilson C, Bushell AC, Cusack S. 2004. *Unified Model Documentation Paper 26. The Large-Scale Cloud Scheme and Saturated Specific Humidity*. Met Office: Exeter, UK.

Wilson DR, Bushell AC, Kerr-Munslow AM, Price D, Morcrette C. 2008a. PC2: A prognostic cloud fraction and condensation scheme. Part I: Scheme description. *Q. J. R. Meteorol. Soc.* **134**: 2093–2107.

Wilson DR, Bushell AC, Kerr-Munslow AM, Price D, Morcrette, C, Bodas-Salcedo A. 2008b. PC2: A prognostic cloud fraction and condensation scheme. Part II: Results of climate model simulations. *Q. J. R. Meteorol. Soc.* **134**: 2109–2125.

Wood, R, Field PR. 2000. Relationships between total water, condensed water, and cloud fraction in stratiform clouds examined using aircraft data. *J. Atmos. Sci.* **57**: 1888–1905.

Woolnough SJ, Blossey PN, Xu K-M, Bechtold P, Chaboureau J-P, Hosomi T, Iacobellis SF, Luo Y, Petch JC, Wong RY, Xie S. 2010. Modelling of convective processes during the suppressed phase of a Madden–Julian oscillation: Comparing single-column models with cloud resolving models. *Q. J. R. Meteorol. Soc.* **136**: 333–353.

Xie S Hume T, Jakob C, Klein SA, McCoy R, Zhang M. 2010. Observed large-scale structures and diabatic heating and drying profiles during TWP–ICE. *J. Climate* **23**: 57–79.

Zhang MH, Lin JL. 1997. Constrained variational analysis of sounding data based on column-integrated budgets of mass, heat, moisture and momentum: Approach and application to ARM measurements. *J. Atmos. Sci.* **54**: 1503–1524.

